Hydroclimatic variability drives submarine groundwater discharge and nutrient fluxes in an anthropogenically disturbed, semi-arid estuary

Audrey R. Douglas[1*], Dorina Murgulet[1*], Paul A. Montagna[2]

[1]Center for Water Supply Studies, Texas A&M University-Corpus Christi, Corpus Christi, Texas, USA 78412

[2]Harte Research Institute for Gulf of Mexico Studies, Texas A&M University-Corpus Christi, Corpus Christi, Texas, USA, 78412

Submitted to:

Science of the Total Environment

Submission Date:

June 10, 2020

Keywords: flood event, semi-arid estuary, nitrogen, submarine groundwater discharge (SGD), Nueces Bay, nitrogen budget

***CORRESPONDING AUTHOR**: Audrey R. Douglas, Center for Water Supply Studies, Department of Physical and Environmental Sciences, Texas, A&M University-Corpus Christi, 6300 Ocean Drive, Corpus Christi, TX 78412; Phone: 361-825-2309; email: adouglas1@islander.tamucc.edu

Graphical Abstract

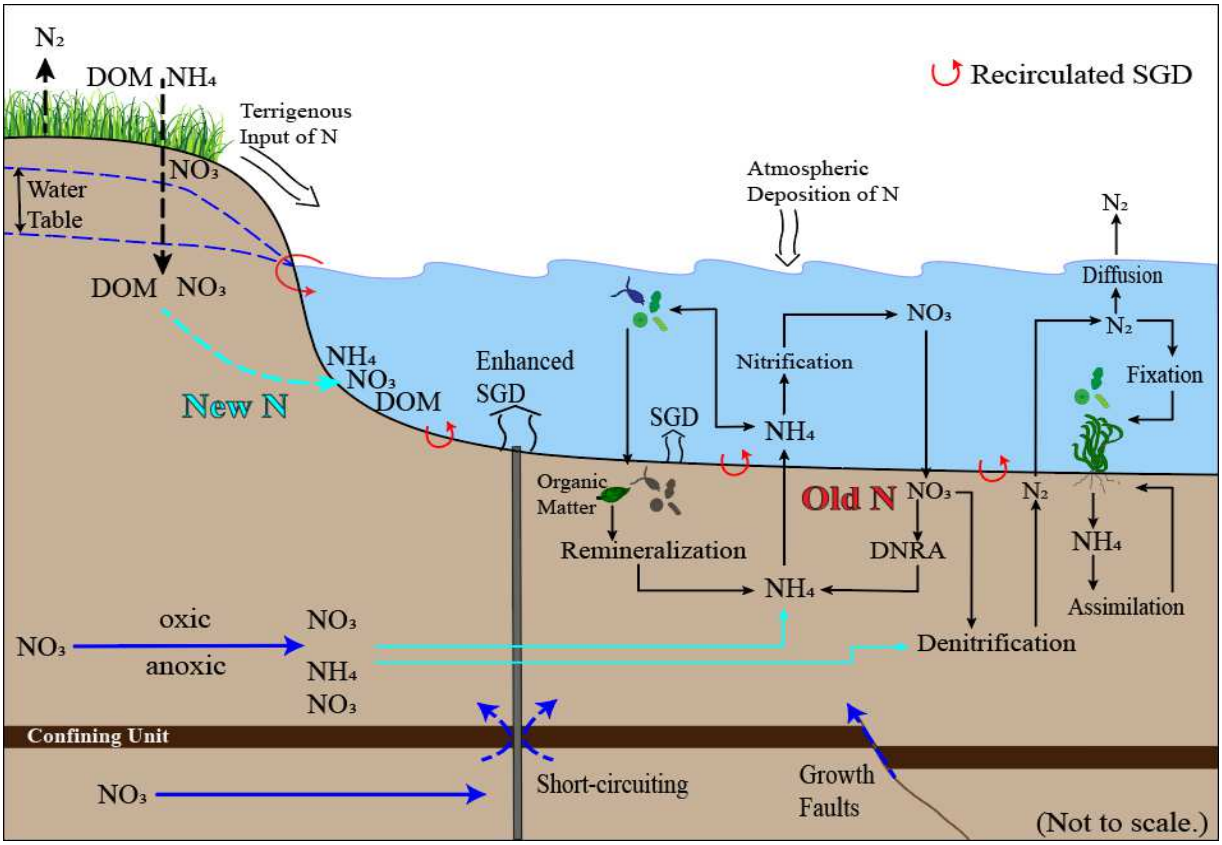

Abstract

Nutrient budgets in semi-arid estuaries, with ephemeral freshwater inflows and limited nutrient sources, are likely incomplete if contributions from submarine groundwater discharge (SGD) are not included. Here, the relative importance of saline/recirculated SGD-derived nutrient fluxes spatiotemporal variability to the overall nutrient budget is quantified for Nueces Bay, Texas, U.S.A., across hydroclimatic conditions ranging from drought to normal, to flood. On average, 67% of the variance in water quality is due to temporal differences while 16% is explained by spatial differences. Principal component analysis (PCA) reveals three principal components: freshwater inflow (PC1 28.8%), saline/recirculated SGD and recycled nitrogen (PC2 15.6%), and total SGD and "new" nitrogen (PC3 11.2%). Total SGD porewater fluxes ranged from 29.9-690.3

mmol·m^{-2}d^{-1} for ammonium, 0.21-18.7 mmol·m^{-2}d^{-1} for nitrite+nitrate, 3.1-51.3 mmol·m^{-2}d^{-1} for phosphate, 57.1-719.7 mmol·m^{-2}d^{-1} for silicate, and 95.9-36,838.5 mmol·m^{-2}d^{-1} for dissolved organic carbon. Total and saline/recirculated SGD fluxes were on average 150 - 26,000 and 5.8 - 466 times, respectively, greater than surface runoff fluxes across all seasons. Nitrogen (N) enrichment in porewater occurs near the agricultural fields because of soil N flushing and percolation to groundwater, which facilitates N-rich groundwater fluxes. There were substantial "new" N inputs from terrestrial groundwater following precipitation while saline/recirculated SGD of recycled N accounts for only <4 % of total SGD inputs. The "new" N inputs occur in the river and river mouth during flooding, and near the north shore where topography and hydraulic gradients are steeper during drought. Thus, while significant inputs of N may be associated with atmospheric deposition, or remineralization in the porewater, groundwater is the highest contributor to the nutrient budget in Nueces Bay. This result implies that nutrient management strategies should focus on land-use practices to reduce N contamination of shallow groundwater and subsequent contamination of estuaries.

1. Introduction

Estuarine eutrophication and hypoxia events have increased as a result of nutrient loading to coastal catchments from human population growth, urbanization, and agricultural and industrial expansion (Bruesewitz et al. 2015; Kennish 2002; Paerl 2009; Scavia and Bricker 2006). As development of coastal regions continues to grow, understanding nutrient inputs and cycling along freshwater-marine gradients is essential to inform nutrient management strategies (Paerl 2009). Along with changing land use, estuaries are influenced by variable hydrological patterns. The patterns of surface runoff and submarine groundwater discharge (SGD) play a critical role in the timing and amount of freshwater, nutrients, organic matter, and sediments delivered to estuaries (Bruesewitz et al. 2015; Mooney and McClelland 2012; Paudel and Montagna 2014; Santos et al. 2013; Urquidi-Gaume et al. 2016). Estuaries in semi-arid regions are subject to sporadic precipitation events that result in generally low riverine inflows and episodic flood events (Montagna and Kalke 1992; Murgulet et al. 2016). Climate projections indicate intensification of periods of drought and episodes of flooding (Stocker 2014; Trenberth et al. 2003). Significant changes in hydrologic conditions are expected with the predicted increase in frequency and intensity of storms as a result of climate change (Rabalais et al. 2009; Stocker 2014), thereby altering patterns of nutrient transport between terrestrial and marine environments.

SGD has been recognized as an important pathway that transports water and solutes from terrestrial to marine environments (Burnett et al. 2003; Moore 2010; Taniguchi et al. 2002). Nutrient input via SGD rivals riverine inputs in some regions and may contribute significantly to nutrient cycling and primary productivity in coastal oceans (Peterson et al. 2008; Slomp and Van Cappellen 2004; Valiela et al. 1990). The potential impact of even a small volume of SGD may be equal to, or greater than, riverine inputs because the concentrations of nitrogen (N) in coastal

groundwater is often much more enriched comparable to surface waters (Valiela et al. 1990). In addition, SGD may play a significant role in nutrient cycling and primary productivity in coastal oceans (Peterson et al. 2008; Slomp and Van Cappellen 2004; Valiela et al. 1990). While additional inputs of nutrients from SGD may be beneficial to the coastal ecology in some areas (Peterson et al. 2008), they were also found to be detrimental when the extent and timing of inputs coincided with harmful algae bloom events (i.e., eutrophication). When in excess, the SGD-derived nutrients can lead to regional increases in primary production, decreases in seagrass beds, and play a role in the extent of coastal hypoxia.

Many studies have assessed the quantity of SGD and the corresponding nutrient fluxes to coastal waters (Charette et al. 2001; Hwang et al. 2016; Luo et al. 2014; Rodellas et al. 2014; Santos et al. 2013; Spalt et al. 2020; Swarzenski et al. 2007; Urquidi-Gaume et al. 2016) or the processes influencing nutrient levels and distributions in surface water (Bruesewitz et al. 2015; Paudel et al. 2019). However, it is likely that groundwater inputs and changes of these fluxes vary at seasonal scales and with extreme hydroclimatic conditions, such as drought and flooding. This research investigated the spatial and temporal changes of inorganic and organic nutrients in a semi-arid estuary relative to the role of SGD-derived nutrients. This study is unique in that it estimated SGD-derived nutrient fluxes based on SGD rates and porewater and groundwater concentrations for a semi-arid estuary across hydroclimatic conditions ranging from drought to flood to "normal" semi-wet conditions. The specific objectives of the present study were to: 1) identify the spatial and temporal changes in inorganic and organic nutrients in semi-arid estuaries across variable hydroclimatic conditions, 2) assess temporal changes in nutrient fluxes to the bay in response to drought, flooding, and typical conditions, and 3) assess the role of SGD-derived nutrients to nutrient budgets under changing hydroclimatic conditions. In addition to a dense spatial sampling

of bay waters, to better constrain the nutrient inputs to the estuary, both river and benthic endmembers were evaluated. The influence of SGD-derived nutrients on the system was evaluated through the application of multivariate statistics.

2. Methods

2.1 Study Area

Nueces Bay (NB), located on the south Texas Gulf of Mexico coast, is a semi-arid, microtidal, secondary bay in the Nueces Estuary system (**Figure 1**). Nueces Bay is ~75 km^2 in area with an average depth of 0.7 m and no direct connection to the Gulf of Mexico. (Diener 1975; NBBEST 2011). The area is characterized by dry to sub-humid climate with annual precipitation averaging around 76.2 cm and an average evaporation rate of 145 cm (Ockerman 2001; Shafer 1968). Persistent winds (17-18 $km \cdot h^{-1}$) result in a generally well-mixed water column and increased turbidity due to sediment resuspension (Ockerman 2001). The primary source of surface water to Nueces Bay comes from Nueces River; however, low precipitation in the watershed and dams and diversions on the river limit riverine discharge. Thus, the lower Nueces River, below the saltwater barrier dam at Labonte Park (**Figure 1**), received little freshwater inflows throughout most of the year and is tidal influenced. These conditions result in high average salinities and often low nutrient levels (Longley et al. 1994). Entering the study period (December 2014 through August 2016), the southern United States and Mexico were experiencing one of the strongest multi-year (4 - 5 years) droughts on record, which ended in spring 2015 (Murgulet et al. 2017; TWDB 2017). Murgulet et al. (2016) and Douglas et al. (2020) provide more detailed information on hydroclimatic variability and freshwater inflows, and the impact of hydrological alterations on stream and groundwater flow in Nueces River.

Nueces Bay falls within the Gulf Coast Aquifer (**Fig. 1A**), a leaky artesian aquifer with a layered stratigraphy of alternating and intermixed silt, clay, sand, and gravel lenses forming the Chicot, Evangeline, and Jasper aquifers (Ashworth and Hopkins 1995; Shafer 1968; Waterstone and Parsons 2003). Nueces Bay and the surrounding systems are generally in direct contact with the Chicot aquifer, which extends 366 m below ground surface (bgs) (Chowdhury et al. 2004; Mace et al. 2006). Additionally, a considerable amount of water discharges upward from the Evangeline, which extends 793 m bgs, into the Chicot aquifer in southern Texas. Most shallow groundwater, i.e., <150 m bgs, in south Texas is brackish to saline with areas of high salinity occurring locally (Kreitler 1993). Generally, hydraulic conditions drive groundwater flows toward the river and the north shore to eventually discharge into the bays and estuaries (Bighash and Murgulet 2015; Breier et al. 2010; Nyquist et al. 2008). Bay surface sediments are predominantly sandy to silty-sand across the north-bay, silty-sand at the Nueces River mouth, clayey-sand to clayey-silt throughout the west-bay and across the south-bay, and silty-clay in the middle of the bay and the lower Nueces River (Shideler et al. 1981). More detailed information about aquifer characteristics are provided elsewhere (Douglas et al. 2020; Waterstone and Parsons 2003; Young et al. 2016).

Previous studies of SGD in this bay by Breier et al. (2010) and Douglas et al. (2020), found similar SGD rates from excess ^{226}Ra but Douglas et al. (2020) found 1-2 orders of magnitude greater SGD rates from excess ^{222}Rn. Further, previous nitrogen budgets for Nueces Estuary and Nueces Bay generated net negative balances (Anchor QEA 2017; Brock 2001); however, these budgets did not account for SGD-derived nitrogen (Brock 2001), nor total nitrogen (Anchor QEA 2017). Thus, the SGD-derived solute fluxes are potentially substantial in semi-arid Nueces Bay.

2.2 Sample Collection and Analysis

This study was conducted from September 2014 through July 2016. Surface water and porewater were sampled quarterly according to the Van Dorn and push-point piezometer methods previously outlined in Murgulet et al. (2018) and Douglas et al. (2020). Water quality variables used for the present study were temperature (temp), salinity (sal, practical salinity scale; the averaged salinity in the global ocean of 35 is used as the reference (Millero 1993)), pH, secchi depth, chlorophyll-α (chl-α), dissolved organic carbon (DOC), total dissolved nitrogen (TDN), ammonium (NH_4^+), nitrate+nitrite ($NO_{2\text{-}3}^-$), orthophosphate (PO_4^{3-}), silicate (SiO_4^{4-}), stable isotopes of nitrate ($\delta^{15}N$ and $\delta^{18}O$), and radioisotopes of radon (^{222}Rn) and radium (^{224}Ra and ^{226}Ra). Details of radioisotope sample collection, sampling stations, water quality parameters, and procedures to measure radioisotopes and water quality parameters are presented in detail elsewhere (Douglas et al. 2020; Murgulet et al. 2018; Nelson and Montagna 2009).

2.2.1 Chlorophyll-α and Nutrients

Surface water samples were filtered (GF/F filter paper) on site and then stored frozen until analysis. Chlorophyll-α was measured with a Turner Design Trilogy fluorometer within 12-16 hours of methanol addition using a methanol extraction method (Krauk et al. 2006; Montagna et al. 2018; Paudel et al. 2019).

Inorganic nutrient measurements were carried out using an OIA Flow Solution autoanalyzer with computer-controlled sample selection and peak processing. The ranges of detection are 0.25-10.0 μM for $NO_{2\text{-}3}^-$, 0.25-10.0 μM for NH_4^+, 0.10-10.0 μM for PO_4^{3-}, and 10.0-300.0 μM for SiO_4^{4-} (Paudel et al. 2019 and references therein). Concentrations in samples exceeding detection limits (i.e., porewaters) were determined through dilution, whereas samples below detection limit were considered as half of the detection limit. DOC and TDN measurements were conducted using a

166 Shimadzu TOC-V analyzer with nitrogen module. Dissolved organic nitrogen (DON) was
167 estimated as the difference between TDN and dissolved inorganic nitrogen (DIN=NO_2^-+NO_3^-
168 +NH_4^+). Ammonium was not removed from TDN samples prior to measurement, thus, only
169 surface water samples, in which ammonium is expected to be relatively low, are used for
170 calculating DON and included in analysis. Only samples with N content ≥0.07 mg·L^{-1} as N were
171 sent for measurement of stable isotopes of nitrate ($\delta^{15}N$ and $\delta^{18}O$). Nitrogen and oxygen isotope
172 ratios of NO_3^- were measured at Colorado Plateau Stable Isotope Laboratory, Northern Arizona
173 University, using the denitrifier method. Nitrite was not removed from these samples; however,
174 NO_3^- and NO_2^- data from this system (Murgulet et al. 2019) shows that NO_2^- accounts for less than
175 21% of NO_2^-+NO_3^- in surface water and less than 14% in porewater. Thus, NO_2^- was interpreted
176 as NO_3^-. Typical standard deviations (1σ) for isotopic measurements are 0.2‰ for $\delta^{15}N$ and 0.5‰
177 for $\delta^{18}O$ (Murgulet and Tick 2013 and references therein).

178 **2.2.2 SGD-derived Nutrient Fluxes**

179 SGD rates, determined from radon and radium mass balances from companion studies
180 Murgulet et al. (2018) and Douglas et al. (2020), were used to calculate the nutrient inputs from
181 total and recirculated/saline SGD. Event average porewater nutrient concentrations (μmol·L^{-1})
182 were multiplied by the SGD rate ($m^3 \cdot d^{-1}$) for each season. Other studies have shown that samples
183 high in ammonium, as expected in porewater (Burdige and Zheng 1998; Murgulet et al. 2019),
184 may create interference during the TDN analysis (Burdige and Zheng 1998). Thus, for assessment
185 of the influence of groundwater fluxes on the nitrogen budget of Nueces Bay, porewater samples
186 from June 2015 through March 2016 were processed to remove NH_4^+. Ammonium was removed
187 from these porewater samples prior to DOC/TDN analysis by: 1) raising the pH of each sample to

188 ~12 with a 10 M NaOH solution, 2) sparging the sample with N_2 gas, and 3) lowering the pH to
189 ~2 with 10 M phosphoric acid for analysis (Burdige and Zheng 1998).

190 **2.3 Statistical Analyses**

191 The goal was to test for spatial differences within the study area over time and different
192 hydroclimatic conditions. Region classifications were predetermined to separate mixing
193 endmembers (i.e., Nueces River [NR], Nueces River mouth [RM], Corpus Christi Bay [CCB]) and
194 spatial variability of sediment types (i.e., north bay silty-sand [NB], mid-bay silty-clay [MB], and
195 west-bay sandy-silt [WB]). Surface water and porewater samples were assessed separately due to
196 an unbalanced number of samples collected for porewater compared to surface water.

197 **3.2.3.1 Principal Components Analysis (PCA)**

198 Principal components analysis (PCA) was performed to analyze the relationship between
199 inorganic and organic nutrients, SGD tracers, and other water quality parameters. PCA allows for
200 the reduction of complex multivariate datasets into smaller more manageable datasets by analyzing
201 inter-correlations among observed variables, or scores, and extracting latent factors that better
202 explain the underlying processes responsible for the variations observed (Bighash and Murgulet
203 2015; Murgulet et al. 2015). Factors are extracted in the order of importance based on the weight,
204 or eigen-value, of each factor on the overall model. Generally, only factors with eigen-values
205 greater than 1 are considered. The results are presented graphically as vector plots in which the
206 position and length of each vector represents the relationship and weight of that variable to the
207 defined latent factor. The closer the vectors are aligned to an axis, the more that vector's variable
208 is correlated with the factor represented on that axis (Murgulet et al. 2015). Most statistical
209 analyses were run using SAS software suite (SAS 2017). Before the analysis, data were
210 standardized to a normal distribution using PROC STANDARD so that scales were the same for

211 all variables. PCA was performed using the PROC FACTOR procedure (Paudel et al. 2019) in
212 principal components mode with VARIMAX rotation for axis rotation.

213 3.2.3.2 Analysis of Variance (ANOVA)

214 A two-way ANOVA was performed to analyze variations in the inorganic and organic
215 nutrients, and hydroclimatic and SGD indicators (i.e., salinity, Rn, and Ra) between different
216 regions within the bay. Samples were collected from stations within each region as defined earlier;
217 thus, stations are nested within the regions. The experimental design is partial-hierarchical two-
218 way ANOVA that can be described by the following statistical model: $Y_{ijkl} = \mu + \alpha_j + \beta_k + \alpha\beta_{jk} +$
219 $\gamma_{k(l)} + \varepsilon_{(i)jkl}$, where Y_{ijkl} is the dependent response variable; μ is the overall sample mean; α_j is the
220 main fixed effect for sampling date where j = 1 to 8; β_k is the main fixed effect for region where k
221 = 1 to 6 for either NR, RM, WB, MB, NB, or CCB; $\alpha\beta_{jk}$ is the main fixed effect for the interaction
222 between dates and regions; $\gamma_{k(l)}$ is the main effect for stations that are nested (or unique) to the
223 regions and are thus a random effect as denoted by the parentheses around the subscript l that
224 represents the 15 stations; $\varepsilon_{(i)jkl}$ and in the random error term for each of the i measurements within
225 cells. This model was computed using PROC GLM. The expected mean squares (EMS), variance
226 components, and correct F-tests were also computed because this is a mixed model. The F-test for
227 date, date*region interaction, and station(region) is formed by dividing the EMS for the main
228 effects by the mean square error. The F-test for the regions is formed by dividing the EMS for the
229 main effect by the sum of EMS of the station effect and the mean square error.

230 A one-way model was applied to the porewater samples from each station and between each
231 sampling event, where sampling data was the main effect and stations were the replicates. A Tukey
232 post hoc multiple comparisons test was performed to identify the difference among group means.

233 Pearson's correlation was performed between nutrients and hydroclimatic and SGD indicators to
234 assess the link between these variables.

235 **3. Results**

236 **3.1 Surface Water Salinity, Nutrients, and Chlorophyll-α**

237 Salinities were different seasonally and spatially (ANOVA, $p < 0.0001$). The results of the
238 Tukey test confirmed the major hydroclimatic events as defined, i.e., the prior drought (September
239 2014 and December 2014), flood (June 2015), and normal designations (April 2015, September
240 2015, December 2015, March 2016). Though June 2016 is different from the other seasons in the
241 normal designation (Tukey Test), this is due to the considerably lower salinities in the river (0.91
242 – 7.41; **Figure 2E**) following some moderate precipitation events. However, the bay salinities are
243 in the same range as the other seasons in the normal designation. Across all seasons, Nueces River
244 salinities were substantially lower than any bay regions by 1.5 to 21 times.

245 The first three principal components, PC1, PC2, and PC3, explained 28.8%, 15.6%, and
246 11.2%, respectively, of the variation in surface water in all seasons for a total of 55.5% of the
247 variability (**Figure 2**). PC1 had temperature, chl-α, PO_4^{3-}, SiO_4^{4-}, and DOC that were inversely
248 correlated with salinity (**Figure 2A, 2D**). Thus, PC1 represents freshwater inflow such that when
249 river discharge rates are high, salinity is low, and nutrient concentrations are high. PC2 revealed
250 that AR, DON and NH_4^+ are inversely correlated to pH (**Figure 2A**). Thus, PC2 represents recycled
251 or "old" N as AR represents the saline/recirculated component of SGD and DON and NH_4^+ are the
252 reduced species of N. PC3 revealed that Rn and $NO_{2\text{-}3}^-$ are positively correlated to each other
253 (**Figure 2D**). Thus, PC3 represents the "new" N as Rn represents total SGD (i.e.,
254 terrestrial+recirculated or fresh+saline) which brings $NO_{2\text{-}3}^-$ directly into the system or converts
255 NH_4^+ to $NO_{2\text{-}3}^-$ through nitrification in the more oxic top few mm of the sediment layer when the

bottom water column is oxic (Jäntti and Hietanen 2012) or through ammonium oxidation coupled to Mn reduction (i.e., anoxic nitrification) (Mortimer et al. 2004). The June 2015 flood event and NR samples have the highest PC1 scores and are followed in magnitude by September 2015 flooding recession, whereas the NB, MB, and CCB regions exhibit the lowest PC1 scores, which indicates that freshwater inflow had the greatest effect in the tidal river and during flooding (**Figure 2B, 2C**). Samples from before the flood event (i.e., September 2014, December 2014, and April 2015) had higher PC2 scores compared to samples following the flood event (i.e., September 2015, December 2015, and March 2016), which indicates greater contributions of "old" N and saline/recirculated SGD before flooding than following flooding. December 2014, June 2015, December 2015, and June 2016 had the higher PC3 scores, particularly in NR and NB, compared to scores for April 2015, September 2015, and March 2016, particularly in CCB, NB, and MB, indicating that the total SGD and "new" N are greater in the river and nearer shore than further offshore in the bay (**Figure 2E, 2F**).

There were temporal differences for all variables (**Table 1A and Figure 3**). For all variables except, pH, NH_4^+, ^{224}Ra, ^{226}Ra, and radium activity ratios, there were spatial differences. Within regions, there were differences by station for temperature, salinity, chl-α, TDN, DON, NH_4^+, PO_4^{3-}, SiO_4^{4-}, Rn, ^{224}Ra, and ARs, but not for secchi, DOC, $NO_{2\text{-}3}^-$, and ^{226}Ra (**Table 1A**). Temperature, which varies seasonally, had 99% of its variation explained by season (**Table 1B**). All other variables had at least 49% of their variability explained by sampling date except for $NO_{2\text{-}3}^-$ (21%). Overall, the average variance explained by date was 67%, by region was 14%, and by station was 8%. Thus, spatial variance is responsible for approximately 22% of all variability on average, which is one-third of the variability accounted for by temporal variance. Therefore, temporal

278 variance exhibits greater control on discharge and geochemical perturbations in semi-arid
279 estuaries.

280 Surface water NH_4^+ concentrations ranged from below detection limit (0.25 µmol·L^{-1}) to 10.7
281 µmol·L^{-1} ($\bar{x}$ = 2.02 µmol·L^{-1}; n=222; **Figure 3A**) and there was no relationship with salinity.
282 Generally, CCB had the lowest NH_4^+ concentrations, though concentrations increased in
283 December 2015 and March 2016. All other regions followed similar trends with the greatest NH_4^+
284 concentrations occurring in April 2015 and June 2016 following moderate precipitation. The RM
285 also experienced elevated NH_4^+ concentrations in December 2014.

286 Nitrite plus nitrate ($NO_{2\text{-}3}^-$) concentrations ranged from below detection limit (0.25 µmol·L^{-1})
287 to 45.2 µmol·L^{-1} ($\bar{x}$ = 1.97 µmol·L^{-1}; n=230; **Figure 3B**) and were generally < 2 µmol·L^{-1}. $NO_{2\text{-}3}^-$
288 concentrations show no relationship to salinity (**Figure 4B**). The highest $NO_{2\text{-}3}^-$ concentrations
289 were measured in NR over three consecutive events: June 2015 (10.1 µmol·L^{-1}), September 2015
290 (12.3 µmol·L^{-1}), and December 2015 (27.6 µmol·L^{-1}). The RM and NB also had slightly elevated
291 $NO_{2\text{-}3}^-$ concentrations in December 2014 (3.6 µmol·L^{-1} and 3.9 µmol·L^{-1}, respectively) and NR
292 again in June 2015 (6.0 µmol·L^{-1}). Stable isotopes of NO_3^- show large enrichment in $\delta^{18}O$ during
293 drought, which is an indication of wet/dry deposition (**Figure 5A**), compared to the relatively
294 lower $\delta^{18}O$ during flooding and normal conditions. Furthermore, a plot of $\delta^{15}N$ vs. 1/[$NO_{2\text{-}3}^-$]
295 (**Figure 5B**) shows that most drought samples plot near the mixing trend indicating that
296 atmospheric deposition may be influential on $NO_{2\text{-}3}^-$ concentrations. However, there were large
297 deviations from mixing in the north bay during drought that may indicate groundwater input may
298 originate from anoxic sediments where nitrification/denitrification, with some anammox, is
299 occurring (Granger and Wankel 2016), or reflect a greater influence of NO_2^- fractionation in these
300 low $NO_{2\text{-}3}^-$ concentration samples. The strong positive correlations during flood (r = 0.95, p =

0.0003) and normal conditions (r = 0.64, p = 0.003) with positive slopes (0.65 and 0.48, respectively) indicate denitrification conditions or that these processes are actively occurring (Granger and Wankel 2016; Kendall et al. 2007).

Surface water PO_4^{3-} concentrations ranged from 0.14 µmol·L^{-1} to 18.2 µmol·L^{-1} ($\bar{x}$ = 2.40 µmol·L^{-1}; n=229; **Figure 3C**). NR had significantly higher PO_4^{3-} concentrations than the other regions. PO_4^{3-} decreased along increasing salinity gradient (**Figure 4C**) and peaked in all regions during June 2015 flooding. While all other regions' concentrations decreased in September 2015 following flooding, NR's concentration continued to increase until the subsequent December 2015 sampling.

Concentrations of SiO_4^{4-} ranged from 25.7 µmol·L^{-1} to 284.4 µmol·L^{-1} ($\bar{x}$ = 98.9 µmol·L^{-1}; n=230; **Figure 3D**) and like PO_4^{3-}, NR had significantly higher SiO_4^{4-} than the other regions and generally decreased along increasing salinity gradient (**Figure 4D**). However, unlike PO_4^{3-}, there appears to be production of SiO_4^{4-} under drought conditions. SiO_4^{4-} concentrations peaked during flooding in all regions and remained high in NR and RM in September 2015. NR SiO_4^{4-} concentrations were high in June 2016 while concentrations in all other regions remained low.

Surface water DOC concentrations ranged from 254 µmol·L^{-1} to 756.3 µmol·L^{-1} ($\bar{x}$ = 442.2 µmol·L^{-1}; n=212; **Figure 3F**) and were highest in NR and RM and lowest in CCB. Under drought and normal conditions, DOC decreased along an increasing salinity gradient (**Figure 4E**). However, under drought conditions there appears to be production of DOC in the RM, WB, MB, and NB.

Concentrations of DON ranged from 3.88 µmol·L^{-1} to 233.8 µmol·L^{-1} ($\bar{x}$ = 24.3 µmol·L^{-1}; n=202; **Figure 3G**) and were highest in September 2014 and December 2014 under drought conditions and lowest in September 2015 and December 2015 following flooding. DON

concentrations generally decrease along an increasing salinity gradient; however, flood conditions show some dilution in NR and NB (4.79 – 30.3 $\mu mol \cdot L^{-1}$) whereas drought conditions show some input in CCB, NB, WB, and RM (**Figure 4F**).

Chl-α concentrations ranged from 0.6 $\mu g \cdot L^{-1}$ to 103.7 $\mu g \cdot L^{-1}$ ($\bar{x}$ = 12.4 $\mu g \cdot L^{-1}$; n=231; **Figure 3H**) with the highest in NR in September 2015 and under flood recession conditions (**Figure 4G**). Chl-α peaked in all regions of the bay except NR and RM during flooding. Concentrations peaked at RM in September 2014 and 2015 and at WB in March 2016. NB and CCB generally had the lowest chl-α concentrations across all seasons. Chl-α was negatively correlated with salinity and positively correlated with DOC, $NO_{2\text{-}3}^-$, PO_4^{3-}, and SiO_4^{4-}.

Across the sampling dates, PO_4^{3-}, SiO_4^{4-}, and DOC generally decrease linearly with increasing salinity until a salinity of ~33 above which higher nutrient concentrations were observed. These higher concentrations indicate an additional source or lower uptake at the high salinity end (under higher salinity ranges) (**Figure 4**). In contrast, NH_4^+, $NO_{2\text{-}3}^-$, and DON exhibit no pattern with salinity.

3.2 Porewater Salinity and Nutrients

Porewater salinities ranged from 23.6 – 40.8 and distributions were not different ($p = 0.52$) across sampling events. The lowest porewater salinities occurred in the river at the station further downstream (station 14) in September 2015 and near the river mouth (stations 8 and 9) in December 2014 and June 2015. The RM porewater salinity (25.4) in December 2014 was lower than the surface water (34.5), supporting the increased fresher groundwater input shown in the PCA. While the low porewater salinities in June (25.1) and September 2015 (23.6) are much higher than the corresponding surface water (1.1 – 1.6 and 10.4 – 13.8, respectively), these low salinity porewaters correspond to high PC3 scores indicating greater influence from fresh groundwater

than from recirculated fresh surface water. The highest porewater salinities occurred at the river station furthest upstream (station 15), in the north bay (stations 1 and 3), and in the west-bay (station 11). Within the bay, average porewater salinities were lowest in June 2015 ($\bar{x}$ = 29.2), March 2016 ($\bar{x}$ = 30.1), and December 2014 ($\bar{x}$ = 30.2) and highest in September 2014 ($\bar{x}$ = 38.7), December 2015 ($\bar{x}$ = 36.8), June 2016 ($\bar{x}$ = 35.5), and April 2015 ($\bar{x}$ = 34.9).

Distributions of NH_4^+ (32.0 – 896.0 µmol·L^{-1}, $\bar{x}$ = 198.5 µmol·L^{-1}), PO_4^{3-} (0.72 – 31.8 µmol·L^{-1}, $\bar{x}$ = 13.9 µmol·L^{-1}), and SiO_4^{4-} (95.6 – 443.3 µmol·L^{-1}, $\bar{x}$ = 207.4 µmol·L^{-1}) were similar across events. Temperature (17.4 – 31.4°C, $\bar{x}$ = 24.7°C, $p < 0.0001$), DOC (69.3 – 15,243.5 µmol·L^{-1}, $\bar{x}$ = 909.2 µmol·L^{-1}, $p < 0.0001$), and $NO_{2\text{-}3}^-$ (BDL – 167.0 µmol·L^{-1}, $\bar{x}$ = 12.5 µmol·L^{-1}, $p < 0.0002$) distributions were different across events . December 2014 DOC concentrations were two orders of magnitude greater than all other events and 20 times greater than the next highest measurement. The $NO_{2\text{-}3}^-$ concentrations for June 2015 were greater than all events. $NH_4^+/NO_{2\text{-}3}^-$ was lowest in June 2015 (1.6), September 2014 (45.1), and September 2015 (95.8) and highest in March 2016 (1,201.3) and April 2015 (482.3). The ratio of $NH_4^+/NO_{2\text{-}3}^-$ in porewater provides an indication of flushing as higher relative concentrations of $NO_{2\text{-}3}^-$. For instance, lower ratio values reflect shorter residence times and greater inputs from groundwater. On the other hand, lower relative concentrations of $NO_{2\text{-}3}^-$, i.e., higher ratio values, indicate more stagnant, anoxic conditions where DOC and reduced inorganic species (e.g. NH_4^+, Mn^{2+}, Fe^{2+}) may accumulate (Abdulla et al. 2018; Komada et al. 2016; Slomp and Van Cappellen 2004).

3.3 SGD-derived Nutrient Fluxes

Douglas et al. (2020) and Murgulet et al. (2018) found a large range of SGD rates depending on the method used to quantify SGD and due to large variations in the groundwater endmember. This study presents the range of nutrient fluxes calculated from saline SGD (Ra-based) and total

370 SGD (average Rn groundwater endmember), as determined in these companion studies, for
371 average porewater nutrient concentrations and average groundwater concentrations (**Table 2**). Due
372 to the unbalanced spatial spread of porewater nutrient measurements, the event-averaged
373 porewater nutrient concentrations were used. No SGD rates were calculated from ^{222}Rn for
374 September 2014 or for Ra for June 2015; thus, no solute fluxes are provided for these events with
375 the corresponding parameters.

376 As total SGD was 1-2 orders of magnitude greater than the saline SGD rates, the resulting
377 total nutrient fluxes were also up to several orders of magnitude greater than the saline nutrient
378 fluxes (**Table 2 and Figure 6**). Total fluxes for DOC, NH_4^+, PO_4^{3-}, and SiO_4^{4-} were highest in
379 December 2014 and lowest in June 2015 (**Figure 6A, C-E**). In contrast, the highest total flux for
380 NO_{2-3}^- occurred in June 2015 when SGD rates were lowest but porewater NO_{2-3}^- concentrations
381 were highest. NO_{2-3}^- fluxes were also relatively elevated in December 2014. The high NO_{2-3}^- fluxes
382 in June 2015 and December 2014 correspond with NR samples that load positively on PC3 (**Figure**
383 **2B**), indicative of a significant groundwater flux of new N to the river. Following wet conditions,
384 groundwater recharge within the watershed to the surficial aquifer increases leading to enhanced
385 groundwater discharge to the river as the hydraulic gradients are steeper along riverbanks.
386 December 2014 inputs are higher in general due to large SGD rates in the river (Douglas et al.
387 2020). The lowest NO_{2-3}^- fluxes occurred in March 2016 which loads negatively on PC3.

388 For saline fluxes, the highest fluxes for DOC were in December 2014, while PO_4^{3-} and SiO_4^{4-}
389 were highest in April 2015 and elevated in December 2014 and December 2015. The lowest DOC
390 fluxes occurred in March and June 2016. The lowest PO_4^{3-} and SiO_4^{4-} fluxes occurred in September
391 2014 and 2015 and June 2015, respectively. Saline NH_4^+ fluxes were highest in December 2015

and April 2015 and lowest in September 2014. The lowest $NO_{2\text{-}3}^{-}$ fluxes were in March 2016, whereas the highest $NO_{2\text{-}3}^{-}$ fluxes occurred in December 2015.

Porewater fluxes were greater than groundwater fluxes across all seasons for DOC, NH_4^+, and PO_4^{3-} while SiO_4^{4-} porewater fluxes were less than groundwater fluxes across all seasons. June 2015 was the only time $NO_{2\text{-}3}^{-}$ fluxes from porewater exceeded fluxes from groundwater, indicative of either $NO_{2\text{-}3}^{-}$ accumulation or production in the porewater or a groundwater source not accounted for, such as from the agricultural area to the north.

4. Discussion

4.1 Relationship Between Nutrients, Chlorophyll-α, and SGD Tracers

As a result of extreme changes in hydroclimatic conditions, temporal fluctuations in freshwater inflows were important drivers of differences in hydrologic and salinity regimes and nutrient sources and fate over the study period. As observed in other estuaries across the northwest Gulf of Mexico coast (Montagna et al. 2018), Nueces Bay experienced a significant drop in salinity due to higher precipitation and subsequent freshwater inflow following the spring-summer 2015 flood event. These lower salinities during flooding were associated with higher concentrations of major inorganic nutrient species ($NO_{2\text{-}3}^{-}$, PO_4^{3-}, SiO_4^{4-}) and DOC (**Figure 3**). A smaller drop in salinity was observed in spring-summer 2016 with a smaller increase in inorganic N nutrients in the bay. This is consistent with findings in nearby Copano Bay (Mooney and McClelland 2012), a secondary bay in the Mission-Aransas estuary, and other bays along the Texas coast (Montagna et al. 2018), which exhibited ephemeral high inorganic nutrient concentrations following episodic rain events.

Though temporal changes in hydroclimatic conditions and salinity changes accounted for most of the variance observed, spatial variability further explains these temporal processes. For

example, bay concentrations of NO_{2-3}^-, PO_4^{3-}, SiO_4^{4-}, and DOC returned to pre-flood levels relatively quickly following flood recession. On the other hand, river PO_4^{3-}, SiO_4^{4-}, and DOC concentrations remained high 3 months post flooding before returning to baseflow concentrations. However, NO_{2-3}^- concentrations continued to increase and did not return to baseflow concentrations until December 2015, nine months post flooding. This significant increase in NO_{2-3}^- concentrations over several months in the river was accompanied by a peak in Rn activity indicating substantial groundwater contributions of "new" N within the river either directly as NO_{2-3}^- or as NH_4^+ which was converted to NO_{2-3}^- through nitrification once in the more oxic water column. However, while Rn activities were still elevated downstream at RM where SGD rates increased each sampling event after flooding, higher concentrations of NO_{2-3}^- were not observed post flooding, thus, removal of NO_{2-3}^- from the surface water and dilution with lower concentration bay water as riverine discharge decreased was likely. Possible NO_{2-3}^-removal pathways include high denitrification or dissimilatory nitrate reduction to ammonium (DNRA) rates in the river, or microbial uptake or biotic assimilation (Burgin and Hamilton 2007).

In September 2015, NO_{2-3}^- was likely consumed by high primary production as chl-α in the river was the highest observed in this study. Indeed, Murgulet et al. (2018) found aerobic respiration to be the dominant biogeochemical process controlling alkalinity and dissolved inorganic carbon in Nueces Bay in September 2015. However, cooler temperatures and reduced daylight in December 2015 would have reduced primary production allowing for NO_{2-3}^- concentrations to increase in surface water. Furthermore, as the river system returned to baseflow conditions following flooding, riverine discharge became negligible downstream of the saltwater barrier dam (**Figure 1**) and the lower river became tidally dominated. Thus, mixing with lower concentration bay waters also dilutes the high NO_{2-3}^- concentrations near the RM. However,

conservative mixing lines between upstream NR (station 15) and RM show slight addition of $NO_{2\text{-}3}^{-}$ in September 2015 and consumption/removal in December 2015 (**Figure 7**). Thus, dilution alone does not account for the loss of $NO_{2\text{-}3}^{-}$.

Denitrification takes place under anoxic conditions when organic carbon and NO_3^- are available (Jäntti and Hietanen 2012). Anoxic conditions were not observed in surface water; thus, denitrification may be considered an insignificant N sink within these shallow surface waters. Nevertheless, denitrification may be a significant N sink in estuarine porewaters. Rapid denitrification may occur in heterogeneous sediments with a high silt content (25%-80% silt) and low permeability where inefficient mixing allows anoxic zones to form and in the presence of high organic matter content or microbial activity (Sawyer 2015), conditions observed in NR. Thus, NO_3^- may be removed from surface water as it circulates through aquatic sediments (the hyporheic zone) in response to currents, waves, and tides (Cardenas et al. 2008; Sawyer 2015; Triska et al. 1989; Zarnetske et al. 2011). Furthermore, the deviation below the conservative mixing line in December 2015 (**Figure 7**) indicates consumption/removal of $NO_{2\text{-}3}^{-}$, which is likely due to high denitrification rates accompanied by reduced microbial uptake in December 2015. This is further supported by the $\delta^{15}N$ and $\delta^{18}O$ values that follow denitrification trends from soil N during flood and normal conditions (**Figure 5A**) and the $\delta^{15}N$ vs. $1/[NO_{2\text{-}3}^{-}]$ deviating toward denitrification for river stations during normal conditions (**Figure 5B**).

DNRA has similar requirements as denitrification (i.e., anoxic conditions, available nitrate, and organic substrates); however, DNRA is thought to be favored in high-carbon low-nitrate systems while denitrification is favored under high-nitrate low-carbon conditions (Burgin and Hamilton 2007). In estuarine sediments, DNRA competes with denitrification and conserves N as NH_4^+ rather than removing it from aquatic systems as N_2 (Giblin et al. 2013). In December 2014

461 and April 2015, NH_4^+ increased first in the river mouth and then throughout the bay as well while
462 CCB remained low, thus little to no ammonium was exported out of the bay (**Figure 2A**). DNRA
463 can be influenced by anthropogenic NO_3^- input as it can affect N cycling in marsh sediments by
464 stimulating ammonia mineralization in anaerobic conditions (Ma and Aelion 2005). As the bay is
465 bordered by the city of Corpus Christi to the south and agricultural croplands to the north,
466 significant anthropogenic $NO_{2\text{-}3}^-$ and NH_4^+ additions through dry/wet deposition are expected
467 (Kendall et al. 2007; Paerl 1997). Thus, the persistent strong southerly winds throughout most of
468 the year (Ockerman 2001) would favor more urban/industrial deposition, while winter cold fronts
469 would bring more agricultural deposition. Stable isotopes of nitrate indicate dry deposition of NO_3^-
470 may have been a significant source in the bay during drought conditions in Winter 2014 (**Figure**
471 **5A**). Thus, shallow estuaries and tidal flats that occur under reducing conditions and are abundant
472 in organic matter, such as in this study, may favor DNRA, which has been found to have rates as
473 high as denitrification rates in some places, such as nearby Baffin Bay (An and Gardner 2002). In
474 addition to DNRA, ammonification of organic matter within the sediments or photooxidation of
475 organic matter from SGD may also produce NH_4^+ (Sipler and Bronk 2015). However, the rates of
476 NH_4^+ production from these processes are still not well constrained.
477 In June 2015, high $NO_{2\text{-}3}^-$ concentrations were observed in porewater across the bay along
478 with lower dissolved oxygen but no significant change in NH_4^+ concentrations, i.e., conditions
479 favorable to denitrification. Production of total alkalinity in summer, fall, and winter was shown
480 to be driven by SGD and denitrification in the companion study by Murgulet et al. (2018).
481 Denitrification has been shown to be favored over anammox in marine sediments at temperatures
482 above 25°C (Dalsgaard and Thamdrup 2002), as seen in the porewater in June and September.
483 Although this indicates that anammox may have not played a large role in the conversion of

484 NH_4^+ and $NO_{2\text{-}3}^-$ to N_2 during summer flooding in this subtropical estuary, NO_2^- concentrations
485 would be needed to further confirm such processes. In the absence of internal sources, shallow
486 groundwater transport from the agricultural fields north of the bay is deemed to be an important
487 source of $NO_{2\text{-}3}^-$ following reoccurring precipitation events in the months prior.

488 The minor precipitation events that occurred between November 2014 and April 2015 are
489 believed to have transported the $NO_{2\text{-}3}^-$ accumulated through deposition into the sediments thus
490 stimulating DNRA. The accumulated NH_4^+ was then flushed from the sediments into the bay as
491 the unconfined aquifers rising water table increased hydraulic gradients following spring
492 precipitation events. Interestingly, a similar minor increase in $NO_{2\text{-}3}^-$ concentrations accompanied
493 high NH_4^+ concentrations in June 2016, also following minor precipitation events after a dry
494 winter, which indicates the transition from dry to wet conditions may help stimulate DNRA. The
495 following flood event continued to flush the remaining accumulated NH_4^+ and DON from the
496 shallow anoxic sediments while also increasing the terrestrial $NO_{2\text{-}3}^-$ and DOC through surface
497 runoff. Concentrations of $NO_{2\text{-}3}^-$ continued to increase following flooding due to enhanced SGD
498 rates that sustained flushing of the sediments as well as increased input of "new" N from deeper
499 groundwater (Douglas et al. 2020). Nutrients returned to pre-flood levels along with SGD rates by
500 9 months post-flooding.

501 **4.2 Nutrient Fluxes**

502 One of the main challenges in estimating benthic nutrient fluxes is defining the nutrient
503 concentrations that represent the groundwater source as production or consumption along flow
504 paths and/or that are occurring within the bottom sediments (Murgulet et al. 2018; Spalt et al.
505 2020; Urquidi-Gaume et al. 2016). To account for the different SGD types and variable
506 groundwater endmember solute concentrations, this study used both the total and saline SGD rates

507 derived using the average groundwater endmember (Douglas et al. 2020; Murgulet et al. 2018)
508 and the nutrient concentrations from average porewater and average groundwater (> 3m and <
509 100m below ground surface). Douglas et al. (2020) found average porewater Ra activity ratios
510 (AR 6.5) were very similar to the average of all groundwater, including deep (ARs<1) and shallow
511 (ARs>1), activity ratios (AR 6.6) due to source mixing within the sediment. Thus, the average
512 SGD rates derived from the average groundwater endmember and the average porewater nutrient
513 concentrations provide the best representation of the groundwater source. Nevertheless, as
514 porewater was extracted from >20 cm below the sediment-water interface, this study assumes no
515 change in the porewater chemistry throughout the sediment profile. However, looking to the NO_{2-3}^-
516 and NH_4^+ fluxes from the groundwater informs about terrestrial solute contributions to the
517 system. Groundwater is generally a source of oxidized forms of N (i.e., NO_{2-3}^-) (Majumdar and
518 Gupta 2000), which, when transported to the anoxic and organic matter rich subterranean estuaries
519 is likely to be converted to more reduced N species, such as increased NH_4^+ and decreased NO_{2-3}^-
520 concentrations in porewater (Slomp and Van Cappellen 2004).

521 Nutrient fluxes attributed to both total and saline SGD exceeded inputs derived from surface
522 water runoff alone for all seasons (**Figure 6**). Riverine nutrient fluxes into the coastal ocean have
523 long been regarded as the primary source for coastal ecosystems (Jickells 1998; Wang et al. 2018)
524 though SGD nutrient fluxes greater than surface runoff/riverine inputs have been observed in
525 subtropical bays (Lee et al. 2012; Wang et al. 2017) and oceanic islands (Stewart et al. 2018).
526 However, the total SGD nutrient fluxes in this study are one to three orders of magnitude greater
527 than in the literature while the saline fluxes are of similar magnitudes (**Table 3**). The June 2015
528 flood and June 2016 moderately wet periods are the only times nutrient fluxes from surface runoff
529 approach fluxes from SGD due to the orders of magnitude greater volume of river discharge. There

530 is generally large separation between total SGD and saline nutrient fluxes. Saline solute fluxes
531 account for less than 4% of the total solute fluxes using the average groundwater endmember SGD
532 rates, and less than 14% using the most conservative total SGD estimates. Furthermore, similar
533 flux ranges of $NO_{2\text{-}3}^-$ and NH_4^+ with different dominant groundwater endmember fluxes reflects
534 the conversion of the considerable supply of $NO_{2\text{-}3}^-$ in groundwater to NH_4^+ within the subterranean
535 estuary. The only nutrients with consistently higher concentrations in groundwater than porewater
536 are $NO_{2\text{-}3}^-$ and SiO_4^{4-}, resulting in greater fluxes from groundwater than in porewater (**Figure 6B,**
537 **6C**). However, considering the large scale of nutrient fluxes, SiO_4^{4-} is the only solute exhibiting
538 little difference between the groundwater and porewater concentrations due to its conservative
539 nature. Thus, there is significant terrestrial input to the system, which is likely due to enhanced
540 groundwater flow from short circuiting around oil/gas wells and pipelines, growth faults, and steep
541 topography along the north shore (Douglas et al. 2020). In comparison, DOC and PO_4^{3-} have
542 greater fluxes from porewater than groundwater likely due to burial of organic matter, P desorption
543 from sediments under anoxic conditions, mineralization of P from organic matter within the
544 sediments in porewater, and P precipitation under oxic conditions within the aquifer (Slomp and
545 Van Cappellen 2004).

546 The high NH_4^+ concentrations in surface water in December 2014 and April 2015
547 correspond with the highest SGD fluxes of NH_4^+ and DOC. The $NO_{2\text{-}3}^-$ fluxes in December 2014
548 and 2015, while elevated compared to $NO_{2\text{-}3}^-$ fluxes for other seasons, were an order of
549 magnitude lower compared to the maximum fluxes during the June 2015 flood event but an order
550 of magnitude greater than the lowest fluxes in April 2015 and March 2016. In contrast, while the
551 $NO_{2\text{-}3}^-$ flux was highest during flood conditions the NH_4^+ flux was the lowest. Thus, the SGD-
552 derived N, and DOC, is more reduced and recycled during drought conditions when nutrient

553 additions from recharge to groundwater are limited and more oxidized or "new" during flooding.
554 Furthermore, the higher porewater NO_{2-3}^- during flooding could indicate more flushing of the
555 sediment as the water table rises and the hydraulic gradient increases. In particular, as discussed
556 above, porewater NO_{2-3}^- was highest in June 2015 in the NB (18 – 179 $\mu mol \cdot L^{-1}$) and are
557 believed to be the result of increased hydraulic gradients following the preceding months' wet
558 conditions, facilitating leaching of N from the surrounding agricultural soils into the unconfined
559 aquifer and transport to the bay. Thus, while the salinity difference between surface water and
560 porewater kept offshore SGD rates low, due to density-difference effects (Santos et al 2012),
561 increased hydraulic gradients and the orders of magnitude higher concentration in porewater are
562 responsible for these high NO_{2-3}^- fluxes. By 3 to 6 months post flooding, deep groundwater
563 signatures were apparent in the porewater (Douglas et al. 2020) and NO_{2-3}^- concentrations had
564 decreased as contamination of deeper groundwater is unlikely and, therefore, this source was
565 likely responsible for diluting shallow groundwater and corresponding NO_{2-3}^- concentrations.

566 **4.3 Implications for Estuarine Nitrogen Budget**

567 Previous nitrogen budgets for Nueces Bay and Nueces Estuary generated net negative
568 balances (Anchor QEA 2017; Brock 2001) indicating more N was leaving the system through
569 diversions, tidal exchange, denitrification, and nitrogen burial than entering from known sources
570 (i.e., gauged streams, ungauged watersheds, wastewater treatment plants, other return flows,
571 wet/dry deposition, nitrogen fixation, and SGD). However, these budgets either did not account
572 for SGD-derived N (Brock 2001) or estimated SGD-derived N from NO_3^-, and thus likely
573 underestimated the contribution of total N from groundwater (Anchor QEA 2017). This study
574 applied the bay-wide TDN porewater fluxes for June 2015, September 2015, December 2015, and
575 March 2016 from Douglas et al (in prep), which removed ammonium prior to measurement, to the

576 most recent N budget from Anchor QEA (2017) for years 1986-2015. Anchor QEA (2017) had a
577 N budget of -611 10^6 g N·yr^{-1} (million g N·yr^{-1}, after removing the estimated 75 10^6 g N·yr^{-1} from
578 regional groundwater NO_3^- concentrations). This study found total Rn-derived N fluxes ranged
579 from 16.2 – 82.6 10^9 g N·d^{-1} and averaged 45.8 10^9 g N·yr^{-1}. In contrast, the saline Ra-derived N
580 fluxes ranged from 591 – 2313 10^6 g N·d^{-1} and averaged 1.4 10^9 g N·yr^{-1}. These Ra-derived annual
581 average TDN fluxes are up to an order of magnitude greater than those used by Anchor QEA
582 (2017); however, the Rn-derived annual average TDN fluxes are two orders of magnitude greater
583 than the N fluxes Anchor QEA (2017) used.

584 Total N fluxes for the current study are calculated from applying the average SGD flux to the
585 previous N budget. On average, SGD supplies more N to the system than accounted for by all
586 estimated inputs and sinks creating an excess of 45.2 10^9 g N·yr^{-1}. Nitrogen fluxes could be over
587 3 times greater by applying the SGD rate using the average porewater endmember (i.e., least
588 conservative SGD rates) or 3.5 times less with the SGD rate using the highest groundwater
589 endmember (i.e., most conservative SGD rates) than the average groundwater endmember SGD
590 rates provide. However, even these most conservative total fluxes and the significantly smaller
591 saline/recirculated fluxes generate a substantial surplus of N (4.6 – 23.6 10^9 g N·yr^{-1} and 0.8 10^9 g
592 N·yr^{-1}, respectively) to the system which may have considerable impacts on microbial and
593 planktonic communities within the larger Nueces Estuary.

594 This study provides critical information for the development of appropriate and necessary
595 mitigation strategies required to maintain the estuarine health. With the groundwater input the
596 most significant in this estuary, efforts should be directed at mitigating groundwater pollution.
597 For integrated management measures, further investigations of N levels and sources in
598 groundwater within the watershed, as well as a deeper understanding of the hydrologic system

599 combined with local farmers and stakeholders participation is necessary (Nerantzis et al. 2020).
600 To aid development of rational N management strategies, future studies should incorporate
601 mathematical prediction of nutrient concentrations with assessments of the hydrogeochemical
602 processes to better understand how water quality parameters within an aquifer interact (Bui et al.
603 2020).

604 **5. Conclusions**

605 Assuming the results in Nueces Bay are typical of semi-arid bays, then the temporal change
606 in hydroclimatic conditions and freshwater inflows have significant impacts on the delivery of
607 nutrients to semi-arid estuaries and relatively small, shallow bays. Observations of spatial
608 variability of SGD rates and nutrient levels throughout the system over time further elucidate the
609 processes occurring (e.g., nitrification, dentrification, and DNRA) and the relative control that
610 system heterogeneity has on these processes. While overall SGD is inhibited during flooding, N
611 enrichment in porewater occurs particularly near the agricultural fields as a result of soil N
612 flushing and percolation to groundwater, which facilitates N-rich groundwater fluxes. Evidence
613 points to substantial "new" N inputs from terrestrial groundwater to the porewater and then to the
614 bay, while saline/recirculated SGD accounts for a much smaller fraction of total SGD inputs,
615 thereby contributing to the recycled N portion in the system. This study adds to the body of work
616 that has found SGD-derived nutrient fluxes equivalent to or greater than the riverine-derived
617 nutrient fluxes to a system. However, the present study also demonstrates that nutrient fluxes
618 from SGD in semi-arid and anthropogenically disturbed, estuaries may be significant. Thus,
619 increased N and P contamination of groundwater from industrial and agricultural practices may
620 increase occurrences of eutrophication and harmful algal blooms in semi-arid estuaries. Although
621 N inputs from atmospheric deposition or remineralization are important, because groundwater is

622 the highest contributor to the nutrient budget, management strategies should focus on land-use
623 practices to reduce N contamination of shallow groundwater and subsequent contamination of
624 estuaries.
625
626 Acknowledgements
627 Texas Sea Grant (award number NA14OAR4170102) and the Center for Water Supply
628 Studies at Texas A&M University-Corpus Christi financially supported this research and ARD's
629 dissertation from which this paper has been derived. Partial support to PAM for this publication
630 was made possible by the National Oceanic and Atmospheric Administration, Office of
631 Education Educational Partnership Program (award number NA16SEC4810009).The authors
632 thank all those who assisted in the lab and/or in the field. Finally, the authors thank the reviewers
633 for their comments. All views, opinions, findings, conclusions, and recommendations expressed
634 in this material are those of the authors and do not necessarily reflect the opinions of the Texas
635 Sea Grant College Program or the U.S. Department of Commerce, National Oceanic and
636 Atmospheric Administration.
637
638

639 REFERENCES

640 Abdulla, H. A., D. J. Burdige & T. Komada, 2018. Accumulation of deaminated peptides in
641 anoxic sediments of Santa Barbara Basin. Geochimica et Cosmochimica Acta 223:245-
642 258.
643 An, S. & W. S. Gardner, 2002. Dissimilatory nitrate reduction to ammonium (DNRA) as a
644 nitrogen link, versus denitrification as a sink in a shallow estuary (Laguna Madre/Baffin
645 Bay, Texas). Marine Ecology Progress Series 237:41-50.
646 Anchor QEA, 2017. Nutrient Budget for Nueces Bay. vol TWDB Contract# 1600012015.
647 TWDB, Austin, TX.
648 Ashworth, J. & J. Hopkins, 1995. Aquifers of Texas: Texas Water Development Board Report
649 345. Austin.
650 Bighash, P. & D. Murgulet, 2015. Application of factor analysis and electrical resistivity to
651 understand groundwater contributions to coastal embayments in semi-arid and
652 hypersaline coastal settings. Science of the Total Environment 532:688-701.
653 Breier, J. A., C. F. Breier & H. N. Edmonds, 2010. Seasonal dynamics of dissolved Ra isotopes
654 in the semi-arid bays of south Texas. Marine Chemistry 122(1-4):39-50.
655 Brock, D. A., 2001. Nitrogen budget for low and high freshwater inflows, Nueces Estuary,
656 Texas. Estuaries 24(4):509-521.
657 Bruesewitz, D. A., W. S. Gardner, R. F. Mooney & E. J. Buskey, 2015. Seasonal water column
658 NH 4+ cycling along a semi-arid sub-tropical river–estuary continuum: responses to
659 episodic events and drought conditions. Ecosystems 18(5):792-812.
660 Bui, D. T., K. Khosravi, M. Karimi, G. Busico, Z. S. Khozani, H. Nguyen, M. Mastrocicco, D.
661 Tedesco, E. Cuoco & N. Kazakis, 2020. Enhancing nitrate and strontium concentration

662 prediction in groundwater by using new data mining algorithm. Science of The Total
663 Environment 715:136836 doi:https://doi.org/10.1016/j.scitotenv.2020.136836.
664 Burdige, D. J. & S. Zheng, 1998. The biogeochemical cycling of dissolved organic nitrogen in
665 estuarine sediments. Limnology and Oceanography 43(8):1796-1813.
666 Burgin, A. J. & S. K. Hamilton, 2007. Have we overemphasized the role of denitrification in
667 aquatic ecosystems? A review of nitrate removal pathways. Frontiers in Ecology and the
668 Environment 5(2):89-96.
669 Burnett, W. C., H. Bokuniewicz, M. Huettel, W. S. Moore & M. Taniguchi, 2003. Groundwater
670 and pore water inputs to the coastal zone. Biogeochemistry 66(1-2):3-33.
671 Cardenas, M. B., P. L. Cook, H. Jiang & P. Traykovski, 2008. Constraining denitrification in
672 permeable wave-influenced marine sediment using linked hydrodynamic and
673 biogeochemical modeling. Earth and Planetary Science Letters 275(1-2):127-137.
674 Charette, M. A., K. O. Buesseler & J. E. Andrews, 2001. Utility of radium isotopes for
675 evaluating the input and transport of groundwater-derived nitrogen to a Cape Cod
676 estuary. Limnology and Oceanography 46(2):465-470.
677 Chowdhury, A. H., S. Wade, R. E. Mace & C. Ridgeway, 2004. Groundwater availability model
678 of the central gulf coast aquifer system: numerical simulations through 1999. Texas
679 Water Development Board, unpublished report 1:14.
680 Dalsgaard, T. & B. Thamdrup, 2002. Factors controlling anaerobic ammonium oxidation with
681 nitrite in marine sediments. Appl Environ Microbiol 68(8):3802-3808.
682 Diener, R. A., 1975. Cooperative Gulf of Mexico Estuarine Inventory and Study--Texas: Area
683 Description. National Oceanic and Atmospheric Administration, docs.lib.noaa.gov.

684 Douglas, A. R., D. Murgulet & R. N. Peterson, 2020. Submarine groundwater discharge in an
685 anthropogenically disturbed, semi-arid estuary. Journal of Hydrology 580:124369.
686 Giblin, A. E., C. R. Tobias, B. Song, N. Weston, G. T. Banta & V. H. RIVERA-MONROY,
687 2013. The importance of dissimilatory nitrate reduction to ammonium (DNRA) in the
688 nitrogen cycle of coastal ecosystems. Oceanography 26(3):124-131.
689 Granger, J. & S. D. Wankel, 2016. Isotopic overprinting of nitrification on denitrification as a
690 ubiquitous and unifying feature of environmental nitrogen cycling. Proceedings of the
691 National Academy of Sciences 113(42):E6391-E6400.
692 Hwang, D.-W., I.-S. Lee, M. Choi & T.-H. Kim, 2016. Estimating the input of submarine
693 groundwater discharge (SGD) and SGD-derived nutrients in Geoje Bay, Korea using
694 222Rn-Si mass balance model. Marine Pollution Bulletin 110(1):119-126
695 doi:https://doi.org/10.1016/j.marpolbul.2016.06.073.
696 Jäntti, H. & S. Hietanen, 2012. The effects of hypoxia on sediment nitrogen cycling in the Baltic
697 Sea. Ambio 41(2):161-169.
698 Jickells, T., 1998. Nutrient biogeochemistry of the coastal zone. Science 281(5374):217-222.
699 Kendall, C., 1998. Tracing nitrogen sources and cycling in catchments. Isotope tracers in
700 catchment hydrology 1:519-576.
701 Kendall, C., E. M. Elliott & S. D. Wankel, 2007. Tracing anthropogenic inputs of nitrogen to
702 ecosystems. Stable Isotopes in Ecology and Environmental Science, 2nd Edition:375-449
703 doi:DOI 10.1002/9780470691854.ch12.
704 Kennish, M. J., 2002. Environmental threats and environmental future of estuaries.
705 Environmental conservation 29(1):78-107.

706 Komada, T., D. J. Burdige, C. Magen, H.-L. Li & J. Chanton, 2016. Recycling of Organic Matter
707 in the Sediments of Santa Monica Basin, California Borderland. Aquatic Geochemistry
708 22(5):593-618 doi:10.1007/s10498-016-9308-0.
709 Krauk, J. M., T. A. Villareal, J. A. Sohm, J. P. Montoya & D. G. Capone, 2006. Plasticity of N:P
710 ratios in laboratory and field populations of Trichodesmium spp. Aquatic Microbial
711 Ecology 42(3):243-253.
712 Kreitler, C. W., 1993. Geochemical techniques for identifying sources of ground-water
713 salinization. CRC press.
714 Lee, C. M., J. J. Jiao, X. Luo & W. S. Moore, 2012. Estimation of submarine groundwater
715 discharge and associated nutrient fluxes in Tolo Harbour, Hong Kong. Science of the
716 total environment 433:427-433.
717 Longley, W. L., G. L. Powell, A. W. Green & T. W. D. Board, 1994. Freshwater inflows to
718 Texas bays and estuaries: ecological relationships and methods for determination of
719 needs. Texas Water Development Board, Austin, TX.
720 Luo, X., J. J. Jiao, W. S. Moore & C. M. Lee, 2014. Submarine groundwater discharge
721 estimation in an urbanized embayment in Hong Kong via short-lived radium isotopes and
722 its implication of nutrient loadings and primary production. Marine Pollution Bulletin
723 82(1-2):144-154.
724 Ma, H. & C. M. Aelion, 2005. Ammonium production during microbial nitrate removal in soil
725 microcosms from a developing marsh estuary. Soil Biology and Biochemistry
726 37(10):1869-1878 doi:https://doi.org/10.1016/j.soilbio.2005.02.020.

727 Mace, R. E., W. F. Mullican, E. S. Angle, S. C. Davidson & Texas Water Development Board.,
728 2006. Aquifers of the Gulf coast of Texas. Texas Water Development Board, Austin,
729 Tex.
730 Majumdar, D. & N. Gupta, 2000. Nitrate pollution of groundwater and associated human health
731 disorders. Indian journal of environmental health 42(1):28-39.
732 Millero, F. J., 1993. What is PSU? Oceanography 6(3):67-67.
733 Montagna, P. A., X. Hu, T. A. Palmer & M. Wetz, 2018. Effect of hydrological variability on the
734 biogeochemistry of estuaries across a regional climatic gradient. Limnology and
735 Oceanography 63(6):2465-2478.
736 Montagna, P. A. & R. D. Kalke, 1992. The Effect of Fresh-Water Inflow on Meiofaunal and
737 Macrofaunal Populations in the Guadalupe and Nueces Estuaries, Texas. Estuaries
738 15(3):307-326.
739 Mooney, R. F. & J. W. McClelland, 2012. Watershed Export Events and Ecosystem Responses
740 in the Mission–Aransas National Estuarine Research Reserve, South Texas. Estuaries and
741 coasts 35(6):1468-1485.
742 Moore, W. S., 2010. The Effect of Submarine Groundwater Discharge on the Ocean. Annual
743 Review of Marine Science 2:59-88.
744 Mortimer, R. J., S. J. Harris, M. D. Krom, T. E. Freitag, J. I. Prosser, J. Barnes, P. Anschutz, P. J.
745 Hayes & I. M. Davies, 2004. Anoxic nitrification in marine sediments. Marine Ecology
746 Progress Series 276:37-52.
747 Murgulet, D., A. Douglas, C. Lopez, B. Gyawali & V. Murgulet, 2019. Impacts of Temporal and
748 Spatial Variation of Submarine Groundwater Discahrge on Nutrient Fluxes to Texas
749 Coastal Embayments. Texas General Land Office, Austin, TX.

750 Murgulet, D., V. Murgulet, N. Spalt, A. Douglas & R. G. Hay, 2016. Impact of hydrological
751 alterations on river-groundwater exchange and water quality in a semi-arid area: Nueces
752 River, Texas. Science of The Total Environment 572:595-607.
753 Murgulet, D. & G. R. Tick, 2013. Understanding the sources and fate of nitrate in a highly
754 developed aquifer system. Journal of Contaminant Hydrology 155:69-81.
755 Murgulet, D., M. Trevino, A. Douglas, N. Spalt, X. Hu & V. Murgulet, 2018. Temporal and
756 spatial fluctuations of groundwater-derived alkalinity fluxes to a semiarid coastal
757 embayment. Science of The Total Environment 630:1343-1359
758 doi:https://doi.org/10.1016/j.scitotenv.2018.02.333.
759 Murgulet, D., M. Valeriu, R. R. Hay, P. Tissot & A. M. Mestas-Nuñez, 2017. Relationships
760 between sea surface temperature anomalies in the Pacific and Atlantic Oceans and South
761 Texas precipitation and streamflow variability. Journal of Hydrology 550:726-739.
762 Murgulet, D., M. S. Wetz, A. Douglas, W. McBee, N. Spalt & K. Linares, 2015. Evaluating
763 Groundwater Inflow and Nutrient Transport to Texas Coastal Embayments. Texas
764 General Land Office.
765 NBBEST (Nueces River and Corpus Christi and Baffin Bays Basin and Bay Expert Science
766 Team), 2011. Environmental Flows Recommendations Report. Final Submission to the
767 Environmental Flows Advisory Group, Nueces River and Corpus Christi and Baffin Bays
768 Basin and Bay Area Stakeholders Committee, and Texas Commission on Environmental
769 Quality.
770 Nelson, K. & P. A. Montagna, 2009. Causes and Monitoring of Hypoxia in Corpus Christi Bay.
771 Nerantzis, K., M. Ioannis, N. Maria-Margarita, B. Matthias, K. Kyriaki, K. Efthimia, M.
772 Manassis, I. Alexandra, V. George & V. Konstantinos, 2020. Origin, implications and

773 management strategies for nitrate pollution in surface and ground waters of
774 Anthemountas basin based on a δ15N-NO3− and δ18O-NO3− isotope approach. Science
775 of The Total Environment:138211.
776 Nyquist, J. E., P. A. Freyer & L. Toran, 2008. Stream bottom resistivity tomography to map
777 ground water discharge. Ground water 46(4):561-569.
778 Ockerman, D. J., 2001. Water Budget for the Nueces Estuary, Texas, May-October 1998. U.S.
779 Geological Survey.
780 Paerl, H. W., 1997. Coastal eutrophication and harmful algal blooms: Importance of atmospheric
781 deposition and groundwater as "new" nitrogen and other nutrient sources. Limnology and
782 oceanography 42(5part2):1154-1165.
783 Paerl, H. W., 2009. Controlling eutrophication along the freshwater–marine continuum: dual
784 nutrient (N and P) reductions are essential. Estuaries and Coasts 32(4):593-601.
785 Paudel, B. & P. A. Montagna, 2014. Modeling inorganic nutrient distributions among hydrologic
786 gradients using multivariate approaches. Ecological Informatics 24:35-46.
787 Paudel, B., P. A. Montagna & L. Adams, 2019. The relationship between suspended solids and
788 nutrients with variable hydrologic flow regimes. Regional Studies in Marine Science
789 29:100657.
790 Peterson, R. N., W. C. Burnett, M. Taniguchi, J. Y. Chen, I. R. Santos & T. Ishitobi, 2008.
791 Radon and radium isotope assessment of submarine groundwater discharge in the Yellow
792 River delta, China. Journal of Geophysical Research-Oceans 113(C9).
793 Rabalais, N. N., R. E. Turner, R. J. Díaz & D. Justić, 2009. Global change and eutrophication of
794 coastal waters. ICES Journal of Marine Science 66(7):1528-1537.

795 Rodellas, V., J. Garcia-Orellana, A. Tovar-Sánchez, G. Basterretxea, J. M. López-Garcia, D.
796 Sánchez-Quiles, E. Garcia-Solsona & P. Masqué, 2014. Submarine groundwater
797 discharge as a source of nutrients and trace metals in a Mediterranean bay (Palma Beach,
798 Balearic Islands). Marine Chemistry 160:56-66.
799 Santos, I. R., J. de Weys, D. R. Tait & B. D. Eyre, 2013. The Contribution of Groundwater
800 Discharge to Nutrient Exports from a Coastal Catchment: Post-Flood Seepage Increases
801 Estuarine N/P Ratios. Estuaries and Coasts 36(1):56-73 doi:10.1007/s12237-012-9561-4.
802 Sawyer, A., 2015. Enhanced removal of groundwater-borne nitrate in heterogeneous aquatic
803 sediments. Geophysical Research Letters 42(2):403-410.
804 Scavia, D. & S. B. Bricker, 2006. Coastal eutrophication assessment in the United States
805 Nitrogen Cycling in the Americas: Natural and Anthropogenic Influences and Controls.
806 Springer, 187-208.
807 Shafer, G. H., 1968. Ground-water Resouces of Nueces and San Patricio Counties, Texas. U.S.
808 Geological Survey.
809 Shideler, G. L., C. E. Stelting & J. H. McGowen, 1981. Maps showing textural characteristics of
810 benthic sediments in the Corpus Christi Bay estuarine system, South Texas. US
811 Geological Survey, Reston, VA.
812 Sipler, R. E. & D. A. Bronk, 2015. Dynamics of Dissolved Organic Nitrogen. Biogeochemistry
813 of Marine Dissolved Organic Matter, 2nd Edition:127-232 doi:10.1016/B978-0-12-
814 405940-5.00004-2.
815 Slomp, C. P. & P. Van Cappellen, 2004. Nutrient inputs to the coastal ocean through submarine
816 groundwater discharge: controls and potential impact. Journal of Hydrology 295(1-4):64-
817 86.

818 Spalt, N., D. Murgulet & H. Abdulla, 2020. Spatial variation and availability of nutrients at an
819 oyster reef in relation to submarine groundwater discharge. Science of The Total
820 Environment 710:136283.
821 Stewart, B. T., K. R. Bryan, C. A. Pilditch & I. R. Santos, 2018. Submarine groundwater
822 discharge estimates using radium isotopes and related nutrient inputs into Tauranga
823 Harbour (New Zealand). Estuaries and coasts 41(2):384-403.
824 Stocker, T., 2014. Climate change 2013: the physical science basis: Working Group I
825 contribution to the Fifth assessment report of the Intergovernmental Panel on Climate
826 Change. Cambridge University Press.
827 Swarzenski, P. W., C. Reich, K. D. Kroeger & M. Baskaran, 2007. Ra and Rn isotopes as natural
828 tracers of submarine groundwater discharge in Tampa Bay, Florida. Marine Chemistry
829 104(1-2):69-84.
830 Taniguchi, M., W. C. Burnett, J. E. Cable & J. V. Turner, 2002. Investigation of submarine
831 groundwater discharge. Hydrological Processes 16(11):2115-2129 doi:10.1002/hyp.1145.
832 Trenberth, K. E., A. Dai, R. M. Rasmussen & D. B. Parsons, 2003. The changing character of
833 precipitation. Bulletin of the American Meteorological Society 84(9):1205-1218.
834 Triska, F. J., V. C. Kennedy, R. J. Avanzino, G. W. Zellweger & K. E. Bencala, 1989. Retention
835 and transport of nutrients in a third-order stream in northwestern California: Hyporheic
836 processes. Ecology 70(6):1893-1905.
837 Groundwater Database (GWDB) Reports: Water Levels by Aquifer 2017. TWDB (Texas Water
838 Development Board),. https://www.twdb.texas.gov/groundwater/data/gwdbrpt.asp#N.
839 Accessed 2017.

840 Urquidi-Gaume, M., I. R. Santos & C. Lechuga-Deveze, 2016. Submarine groundwater
841 discharge as a source of dissolved nutrients to an arid coastal embayment (La Paz,
842 Mexico). Environmental Earth Sciences 75(2):1.
843 Valiela, I., J. Costa, K. Foreman, J. M. Teal, B. Howes & D. Aubrey, 1990. Transport of
844 Groundwater-Borne Nutrients from Watersheds and Their Effects on Coastal Waters.
845 Biogeochemistry 10(3):177-197.
846 Wang, X., H. Li, J. Yang, C. Zheng, Y. Zhang, A. An, M. Zhang & K. Xiao, 2017. Nutrient
847 inputs through submarine groundwater discharge in an embayment: A radon investigation
848 in Daya Bay, China. Journal of Hydrology 551:784-792
849 doi:https://doi.org/10.1016/j.jhydrol.2017.02.036.
850 Wang, X., H. Li, C. Zheng, J. Yang, Y. Zhang, M. Zhang, Z. Qi, K. Xiao & X. Zhang, 2018.
851 Submarine groundwater discharge as an important nutrient source influencing nutrient
852 structure in coastal water of Daya Bay, China. Geochimica et Cosmochimica Acta
853 225:52-65 doi:https://doi.org/10.1016/j.gca.2018.01.029.
854 Waterstone & Parsons, 2003. Groundwater availability of the central Gulf Coast aquifer--
855 Numerical simulations to 2050, Central Gulf Coast, Texas.
856 Young, S. C., M. Jigmond, N. Deeds, J. Blainey, T. E. Ewing, D. Banerj, D. Piemonti, T. Jones,
857 C. Griffith, G. Martinez, C. Hudson, S. Hamlin & J. Sutherland, 2016. Final Report:
858 Identification of Potential Brackish Groundwater Production Areas-Gulf Coast Aquifer
859 System. Texas Water Development Board, Austin, TX, 636.
860 Zarnetske, J. P., R. Haggerty, S. M. Wondzell & M. A. Baker, 2011. Dynamics of nitrate
861 production and removal as a function of residence time in the hyporheic zone. Journal of
862 Geophysical Research: Biogeosciences 116(G1).

FIGURES

Figure 1: Study Area. A) Inset of Texas, USA with location of the aquifer and watershed. B) Location of sample stations in Nueces Bay, Texas.

Figure 2: Principal components (PC) analysis of water quality and SGD tracers. A) Variable loads for PC1 and PC2. B) Sample scores by region for PC1 and PC2. C) Sample scores by sampling event for PC1 and PC2. D) Variable loads for PC1 and PC3. E) Sample scores by region for PC1 and PC3. F) Sample scores by sampling event for PC1 and PC3. Abbreviations: temp, temperature; sal, salinity; chl-a, chlorophyll-α; doc, dissolved organic carbon; don, dissolved organic nitrogen; NH4, ammonium; NOx, nitrate+nitrite; PO4, phosphate; SiO4, silicate; Rn, radon-222; AR, radium 224:226 activity ratio; CCB, Corpus Christi Bay; MB, mid-bay; NB, north-bay; WB, west-bay; RM, river mouth; NR, Nueces River.

Figure 3: Average concentrations of nutrients and chlorophyll-α by bay region over time compared to salinity. A) Ammonium (NH_4^+). B) Nitrate+nitrite ($NO_{2\text{-}3}^-$). C) Phosphate (PO_4^{3-}). D) Silicate (SiO_4^{4-}). E) Salinity. F) Dissolved organic carbon (DOC). G) Dissolved organic nitrogen (DON). H) Chlorophyll-α (Chl-a). Bay region abbreviations: Nueces River (NR), Nueces River mouth (RM), west bay (WB), middle bay (MB), north bay (NB), and Corpus Christi Bay (CCB).

Figure 4: Concentrations of nutrients and chlorophyll-α by salinity compared to hydroclimatic conditions. A) Ammonium (NH_4^+). B) Nitrate+nitrite ($NO_{2\text{-}3}^-$). C) Phosphate (PO_4^{3-}). D) Silicate (SiO_4^{4-}). E) Dissolved organic carbon (DOC). F) Dissolved organic nitrogen (DON). G) Chlorophyll-α (Chl-a). H) ^{224}Ra:^{226}Ra activity ratio.

Figure 5: Stable isotope values in surface and pore waters and sources. A) Average values of $\delta^{15}N$ and $\delta^{18}O$ of nitrate from various N sources. Regions for N sources are modified from Kendall (1998) and Kendall et al. (2007). 1) Atmospheric NO_3^-. 2) NO_3^- fertilizer. 3) NH_4^+ fertilizer and rain. 4) Soil N. 5) Manure and septic waste. 6) Desert NO_3^- deposits. 7) Marine NO_3^-. The two arrows indicate typical expected slopes for data resulting from denitrification of nitrate with initial $\delta^{15}N = +6‰$ and $\delta^{18}O_{NO3\text{-}} = -9‰$ (Kendall et al. 2007). Typical ranges of $\delta^{18}O$ values produced by nitrification of ammonium and organic matter are -15‰ to 15‰. B) Plot of $\delta^{15}N_{NO3\text{-}}$ vs. $1/[NO_{2\text{-}3}^-]$ for surface water, porewater, and groundwater. Theoretical curves from Kendall et al. (2007) resulting from mixing of two sources of nitrate with different concentrations and from denitrification with two with two different fractionations, where mixing yields a straight line whereas denitrification yields curved lines.

Figure 6: Nutrient fluxes for surface runoff (grey area), total SGD (black/white bars), and saline SGD (grey/white bars) over time. Color patterns reflect the greater fluxes are from average porewater endmember (PW, white with black/grey dots) or average groundwater endmember (GW, grey/black with white dots) A) Dissolved organic carbon fluxes. B) Nitrate+nitrite fluxes. C) Ammonium fluxes. D) Phosphate fluxes. E) Silicate fluxes.

Figure 7: Conservative mixing trends between Nueces River (NR) station 15 and river mouth (RM) for September 2015 and December 2015.

TABLES

Table 1: Results of ANOVA for each variable. (A) Probability (p) values for null hypothesis in the mixed ANOVA. (B) Variance components analysis.

Table 2: Average bay-wide total (Rn) and saline (Ra) nutrient fluxes as $x10^3$ $mol \cdot d^{-1}$ for average porewater nutrient concentrations.

Table 3: Comparison of SGD and solute fluxes in similar coastal and estuarine settings (expressed as $m^3 \cdot m^{-2} d^{-1}$ and $mmol \cdot m^{-2} d^{-1}$, respectively). DIN is NO_2^-, NO_3^-, and NH_4^+ combined.

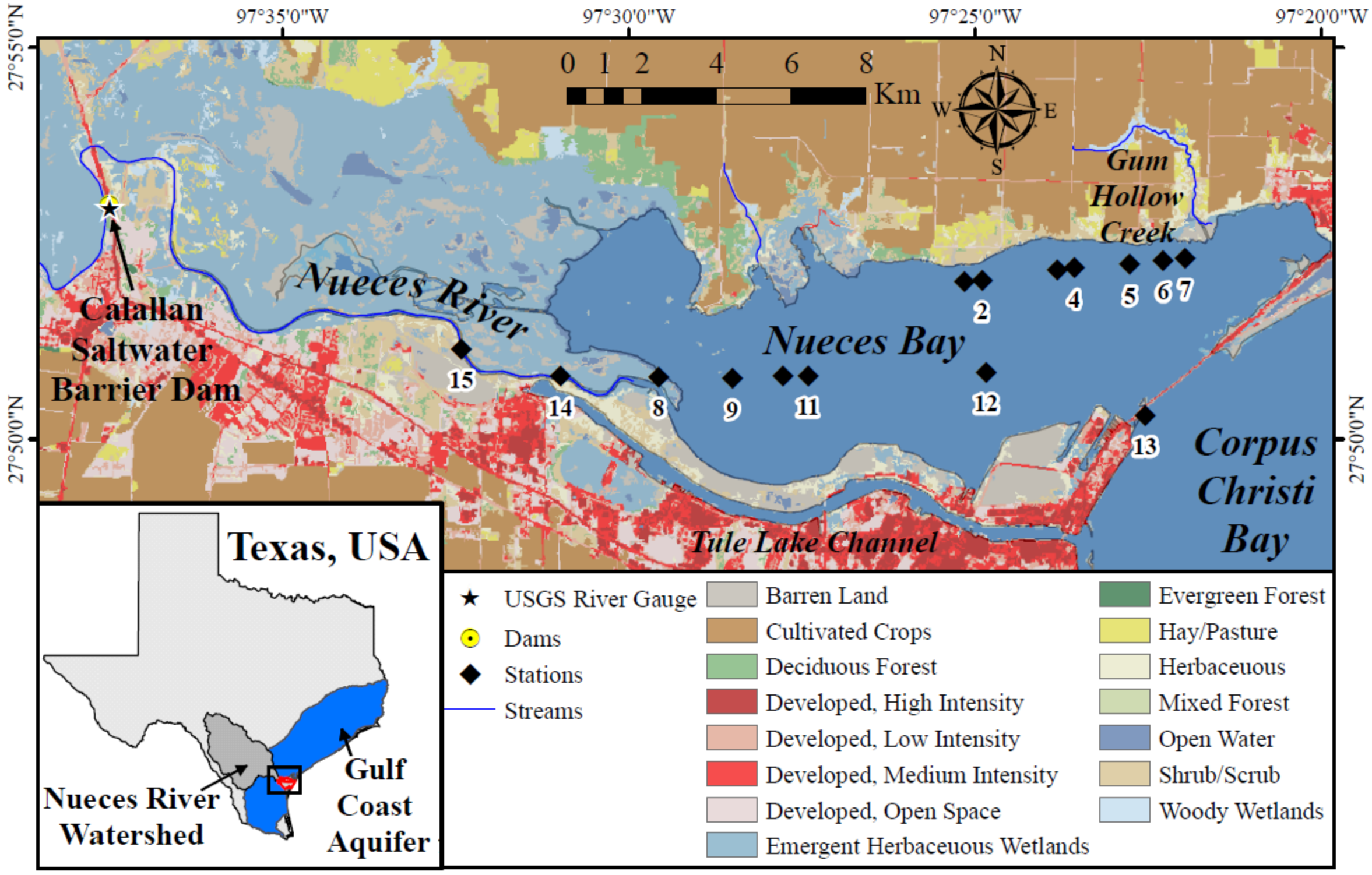
97°35'0"W
97°30'0"W
97°25'0"W
97°20'0"W
27°55'0"N
27°50'0"N
0 1 2 4 6 8
Km
N
W
E
S
Gum Hollow Creek
Nueces River
Nueces Bay
Calallan Saltwater Barrier Dam
Corpus Christi Bay
Tule Lake Channel
2
4
5
6
7
15
14
8
9
11
12
13
Texas, USA
Nueces River Watershed
Gulf Coast Aquifer
USGS River Gauge
Dams
Stations
Streams
Barren Land
Cultivated Crops
Deciduous Forest
Developed, High Intensity
Developed, Low Intensity
Developed, Medium Intensity
Developed, Open Space
Emergent Herbaceuous Wetlands
Evergreen Forest
Hay/Pasture
Herbaceuous
Mixed Forest
Open Water
Shrub/Scrub
Woody Wetlands

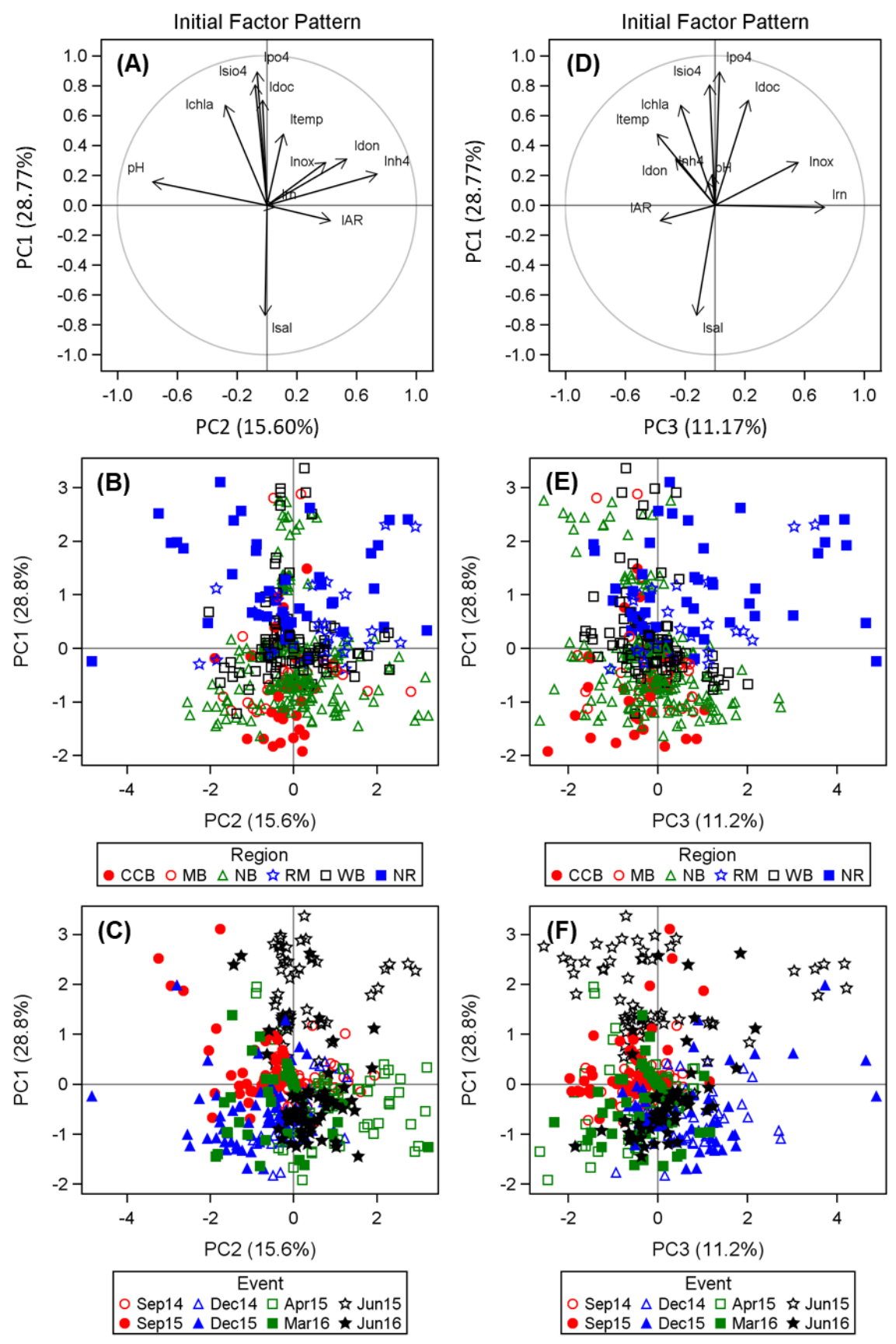
Initial Factor Pattern
(A)
lpo4
lsio4
ldoc
lchla
ltemp
ldon
lnox
lnh4
pH
lrn
lAR
lsal
PC1 (28.77%)
PC2 (15.60%)
Initial Factor Pattern
(D)
lpo4
lsio4
ldoc
lchla
ltemp
lnh4
ldon
pH
lnox
lrn
lAR
lsal
PC1 (28.77%)
PC3 (11.17%)
(B)
PC1 (28.8%)
PC2 (15.6%)
Region
CCB MB NB RM WB NR
(E)
PC1 (28.8%)
PC3 (11.2%)
Region
CCB MB NB RM WB NR
(C)
PC1 (28.8%)
PC2 (15.6%)
Event
Sep14 Dec14 Apr15 Jun15
Sep15 Dec15 Mar16 Jun16
(F)
PC1 (28.8%)
PC3 (11.2%)
Event
Sep14 Dec14 Apr15 Jun15
Sep15 Dec15 Mar16 Jun16

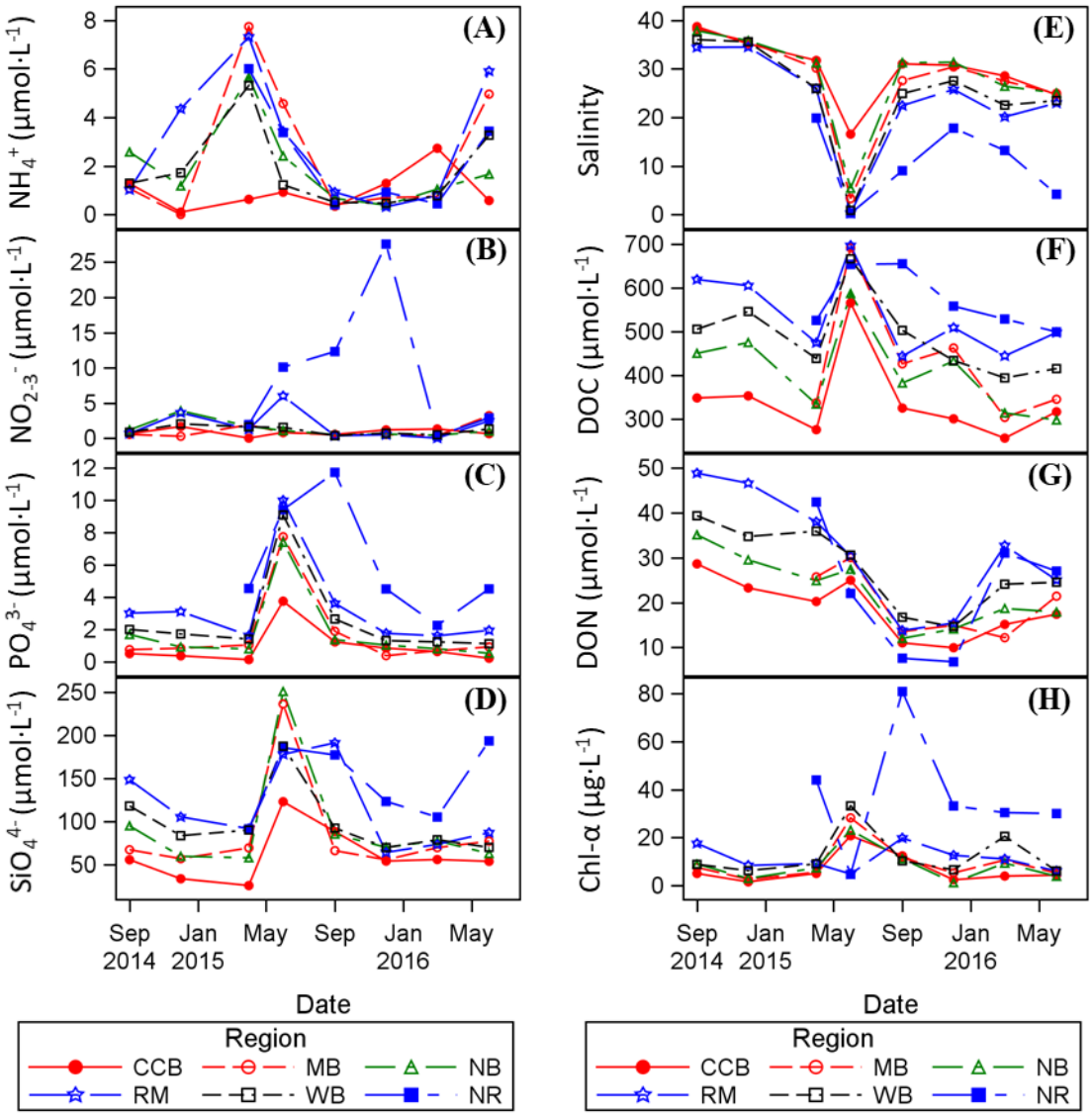
(A)
(B)
(C)
(D)
(E)
(F)
(G)
(H)
NH4+ (µmol·L-1)
NO2-3- (µmol·L-1)
PO43- (µmol·L-1)
SiO44- (µmol·L-1)
Salinity
DOC (µmol·L-1)
DON (µmol·L-1)
Chl-α (µg·L-1)
Sep 2014
Jan 2015
May
Sep
Jan 2016
May
Date
Region
CCB
MB
NB
RM
WB
NR

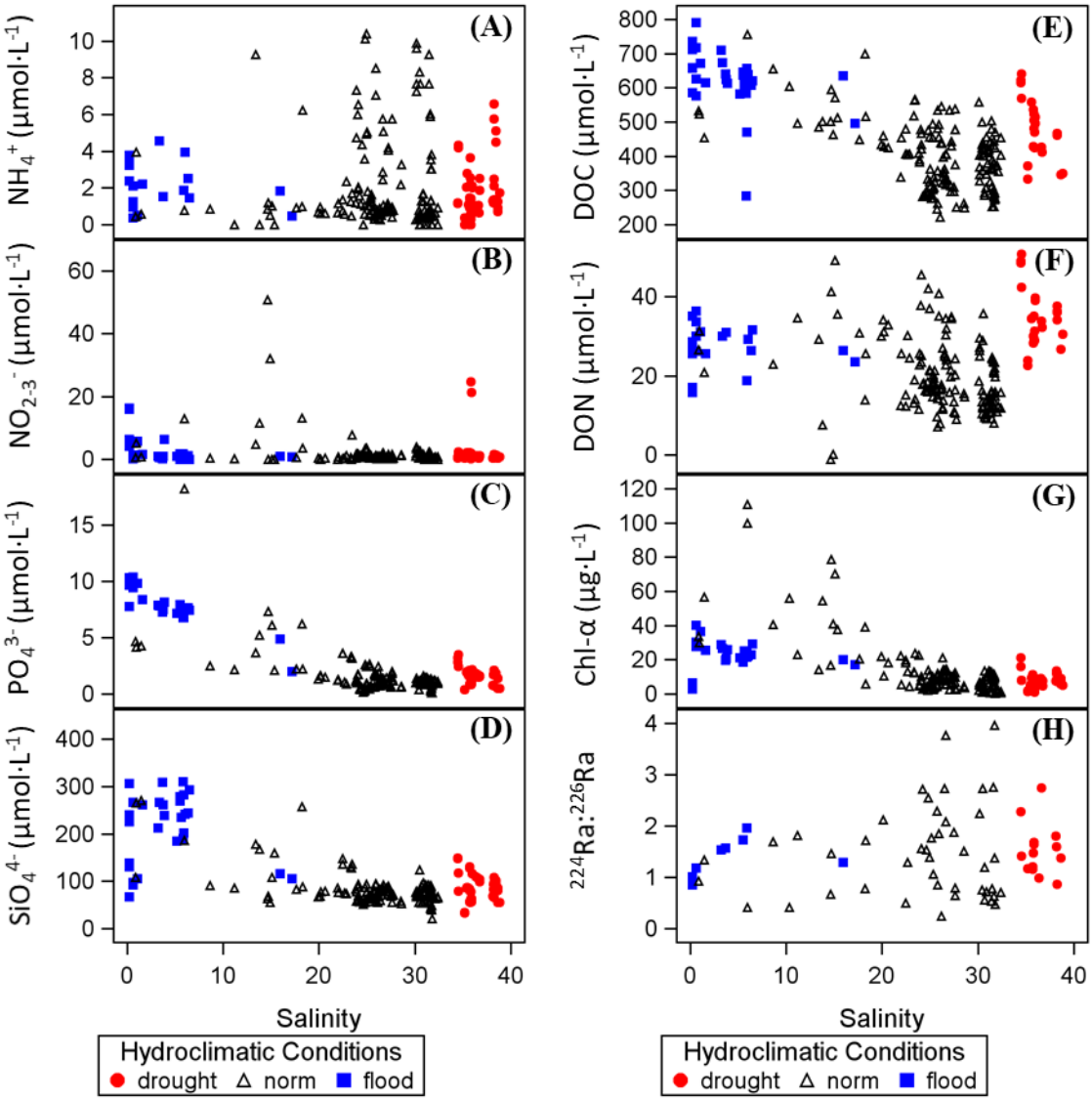
(A)
NH_4^+ (µmol·L^{-1})
(B)
NO_{2-3}^- (µmol·L^{-1})
(C)
PO_4^{3-} (µmol·L^{-1})
(D)
SiO_4^{4-} (µmol·L^{-1})
(E)
DOC (µmol·L^{-1})
(F)
DON (µmol·L^{-1})
(G)
Chl-α (µg·L^{-1})
(H)
^{224}Ra:^{226}Ra
Salinity
Salinity
Hydroclimatic Conditions
drought
norm
flood
Hydroclimatic Conditions
drought
norm
flood

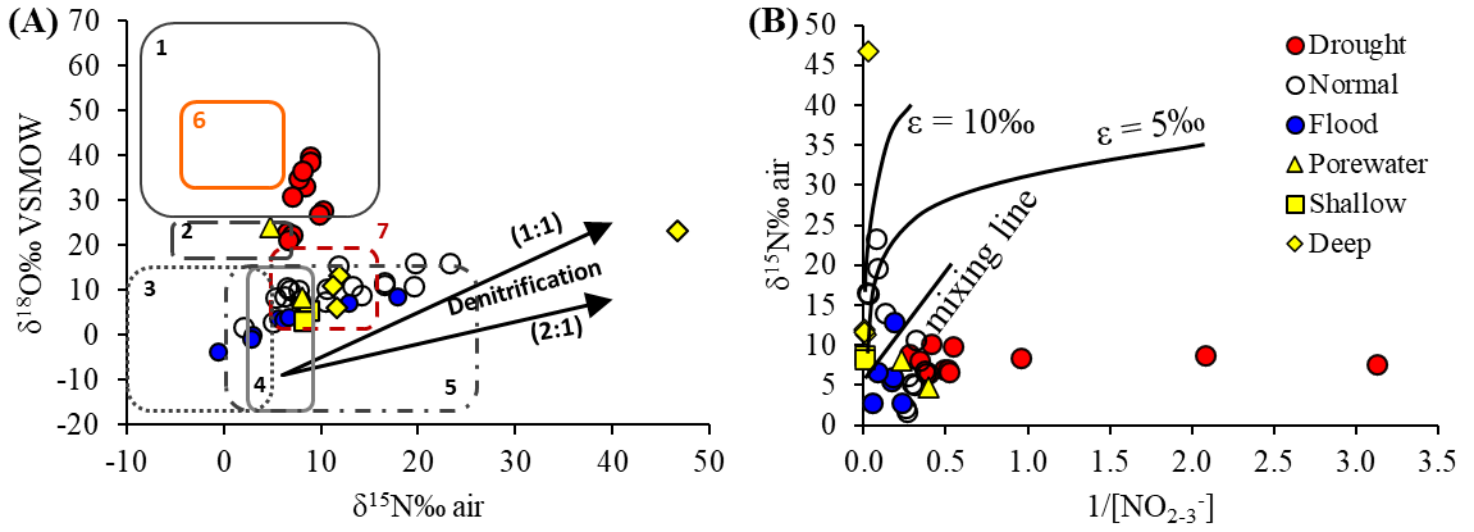
(A)
1
2
3
4
5
6
7
(1:1)
Denitrification
(2:1)
δ18O‰ VSMOW
δ15N‰ air
(B)
ε = 10‰
ε = 5‰
mixing line
δ15N‰ air
1/[NO2-3-]
Drought
Normal
Flood
Porewater
Shallow
Deep

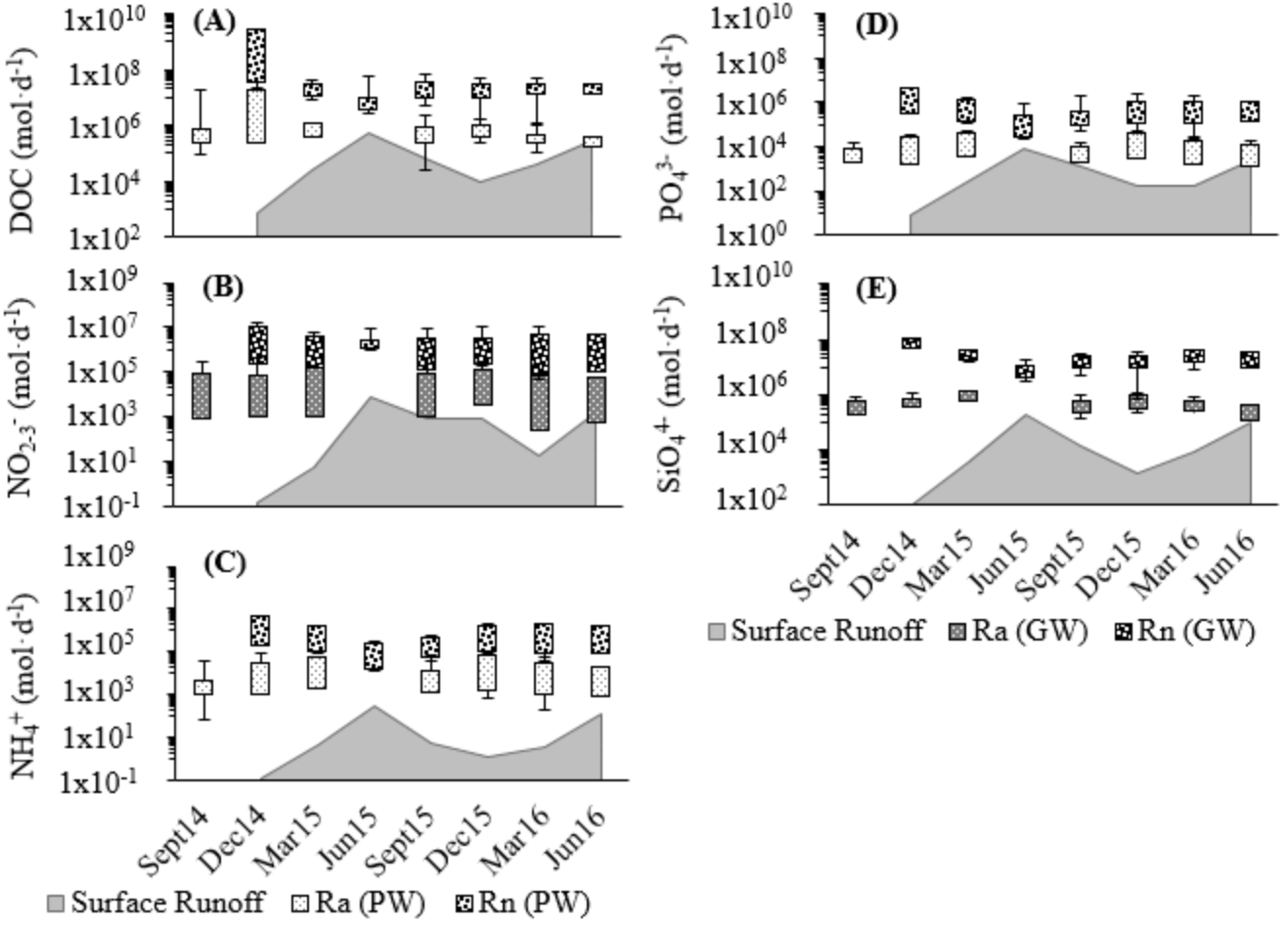
(A)
DOC (mol·d-1)
1x10^10
1x10^8
1x10^6
1x10^4
1x10^2
(B)
NO2-3- (mol·d-1)
1x10^9
1x10^7
1x10^5
1x10^3
1x10^1
1x10-1
(C)
NH4+ (mol·d-1)
(D)
PO43- (mol·d-1)
1x10^0
(E)
SiO4+ (mol·d-1)
Sept14
Dec14
Mar15
Jun15
Sept15
Dec15
Mar16
Jun16
Surface Runoff
Ra (PW)
Rn (PW)
Ra (GW)
Rn (GW)

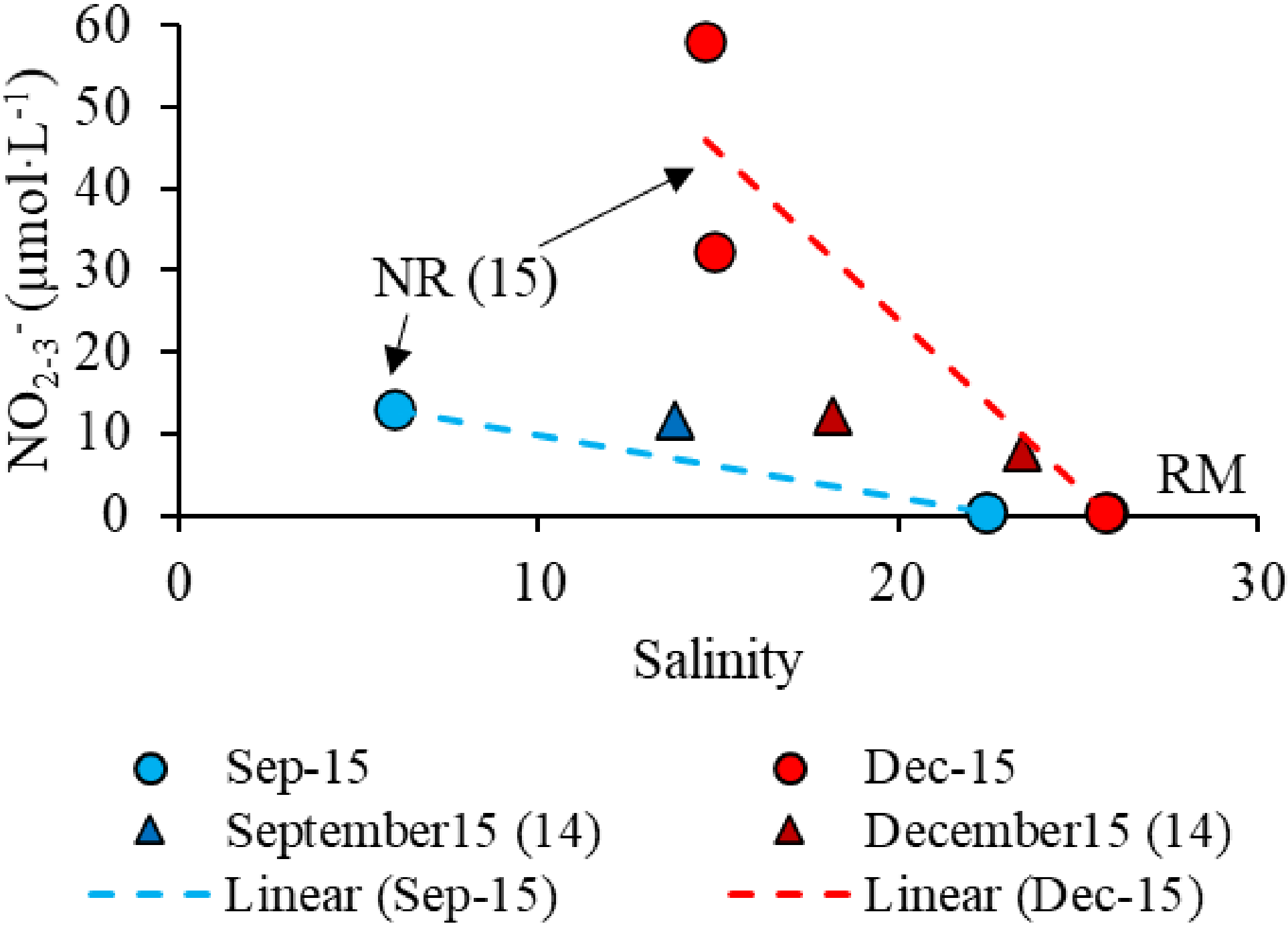
60
50
40
30
20
10
0
NO_{2-3}^{-} (µmol·L^{-1})
NR (15)
RM
0
10
20
30
Salinity
Sep-15
Dec-15
September15 (14)
December15 (14)
Linear (Sep-15)
Linear (Dec-15)

Table 1: Results of ANOVA for each variable. (A) Probability (p) values for null hypothesis in the mixed ANOVA. (B) Variance components analysis.

(A)	**p-values for mixed ANOVA**			
Variable	**Date**	**Region**	**Date *Region**	**Station (Region)**
Temperature	<0.01	0.05	<0.01	0.00
Salinity	<0.01	<0.01	<0.01	<0.01
pH	<0.01	**0.08**	<0.01	<0.01
Secchi	<0.01	0.00	<0.01	**0.18**
Chl-a	<0.01	<0.01	<0.01	<0.01
DOC	<0.01	<0.01	0.03	**0.20**
TDN	<0.01	0.01	**0.06**	0.00
DON	<0.01	0.01	<0.01	0.00
$NO_{2\text{-}3}^{-}$	<0.01	<0.01	<0.01	**0.06**
NH_4^+	<0.01	**0.27**	<0.01	<0.01
PO_4^{3-}	<0.01	<0.01	<0.01	<0.01
SiO_4^{4-}	<0.01	0.00	<0.01	0.03
Rn	<0.01	0.02	0.00	<0.01
Ra-224	<0.01	**0.71**	0.02	0.00
Ra-226	<0.01	**0.17**	0.00	**0.10**
AR	<0.01	**0.43**	**0.75**	0.05
(B)	**Variance components (percent)**			
Variable	**Date**	**Region**	**Date *Region**	**Station (Region)**
Temperature	99	0.3	0.3	0.2
Salinity	92	5	2	1
pH	49	4	37	10
Secchi	60	29	9	2
Chl-a	52	17	26	4
DOC	50	45	2	2
TDN	74	14	4	9
DON	82	9	5	4
$NO_{2\text{-}3}^{-}$	21	50	24	5
NH_4^+	78	2	11	9
PO_4^{3-}	88	7	3	2
SiO_4^{4-}	74	14	9	3
Rn	49	19	9	24
Ra-224	60	2	7	31
Ra-226	84	5	7	3
AR	65	9	5	21
Average	67	14	10	8

Table 2: Average bay-wide total (Rn) and saline (Ra) nutrient fluxes as $x10^3$ $mol \cdot d^{-1}$ for average porewater nutrient concentrations.

		Sept 14	Dec 14	Apr 15	Jun 15	Sept 15	Dec 15	Mar 16	Jun 16
DOC	Rn		$2.61x10^6$	$1.97x10^4$	$6.79x10^3$	$2.38x10^4$	$1.90x10^4$	$1.63x10^4$	$1.57x10^4$
	Ra	483.5	$1.73x10^4$	705.2		602.2	718.4	267.9	199.5
NH_4^+	Rn		$4.89x10^4$	$1.43x10^4$	$2.12x10^3$	$4.29x10^3$	$1.67x10^4$	$1.82x10^4$	$1.55x10^4$
	Ra	38.6	323.6	512.3		108.3	630.8	299.5	196.3
$NO_{2\text{-}3}^-$	Rn		174.0	29.7	$1.32x10^3$	44.7	94.0	15.2	49.8
	Ra	0.9	1.2	1.1		1.1	3.6	0.2	0.6
PO_4^{3-}	Rn		$3.63x10^3$	$1.16x10^3$	221.0	279.4	917.2	912.7	891.9
	Ra	6.8	24.0	41.3		7.1	34.7	15.0	11.3
SiO_4^{4-}	Rn		$5.10x10^4$	$1.76x10^4$	$4.05x10^3$	$8.46x10^3$	$8.44x10^3$	$1.52x10^4$	$8.70x10^3$
	Ra	179.8	337.4	627.8		213.7	319.6	249.4	110.5

Table 3: Comparison of SGD and solute fluxes in similar coastal and estuarine settings (expressed as $m^3 \cdot m^{-2} d^{-1}$ and $mmol \cdot m^{-2} d^{-1}$, respectively). DIN is NO_2^-, NO_3^-, and NH_4^+ combined.

Site	Method	SGD	DOC	DIN	PO_4^{3-}	SiO_4^{4-}	References
Gulf of Aqaba, Israel	^{223,224}Ra mass balance	0.06 - 0.26		2.9 - 10	0.02 - 0.2		Shellenbarger et. al. 2006
Gamak Bay, Korea		0.08 - 0.11		8.8 - 12.1	0.10 - 0.23		Hwang et. al. 2010
Geoje Bay, Korea	^{222}Rn mass balance	0.05		2	0.03	5.9	Hwang et al. 2016
Hampyeong Bay, South Korea	^{226}Ra mass balance	0.14 - 0.35		6.7 - 7.5	0.09 - 0.38	5.5 - 12.9	Waska and Kim 2011
Obama Bay, Japan	^{222}Rn mass balance Salinity mass balance	0.001 - 0.01		0.54	0.02	0.55	Sugimoto et al. 2016
Tolo Harbor, Hong Kong	^{226}Ra mass balance	0.17		21	0.28	27.8	Lee et al. 2014
Tolo Harbor, Hong Kong	^{222}Rn mass balance Ra mass balance Silica mass balance	0.02 - 0.05		2.9 - 6.7	0.02 - 0.12		Luo and Jiao 2016
Tauranga Harbour, New Zealand	^{226}Ra mass balance	0.005 - 0.03		1.07	0.05		Stewart et al. 2018
La Paz Bay, Mexico	^{222}Rn mass balance	0.02 - 0.18		1.5 - 28.2	0.02 - 0.93	6.7 - 95.3	Urquidi-Gaume et. al. 2016
Yucatan Peninsula, Quintana Roo, Mexico	^{223}Ra mass balance Salinity mass balance	48 - 568 2.7 - 8.5		0.002 - 0.01			Null et al. 2014
Hawaii, USA	^{222}Rn mass balance Ra mass balance Silica mass balance	0.02 - 0.65		0.04 - 40	0.01 - 1.6		Street et al. 2008
Huntington Beach, California, USA	Ra mass balance	0.06 - 0.92		0.7 - 12	0.04 - 0.54	-	Boehm et. al. 2004
Turkey Point, Florida, USA	^{222}Rn mass balance	0.11	34.3	5.94	0.35	5.1	Santos et al. 2008
Copano Bay, Texas, USA	^{222}Rn mass balance				0.3 - 3.4	56 - 220	Spalt et al. 2020
Nueces Bay, Texas, USA	^{222}Rn mass balance ^{226}Ra mass balance	0.13 - 3.85 0.01 - 0.39	95.9 - 36,838.5 2.8 - 243.9	30.1 - 709.0 0.54 - 9.0	3.1 - 51.3 0.01 - 0.58	57.1 - 719.7 1.6 - 8.9	This study